NASA Contractor Report 3066

The Flying Hot Wire and Related Instrumentation

Donald Coles, Brian Cantwell,
and Alan Wadcock

GRANT NGL 05-002-229
NOVEMBER 1978

NASA

NASA Contractor Report 3066

The Flying Hot Wire and Related Instrumentation

Donald Coles, Brian Cantwell,
and Alan Wadcock
California Institute of Technology
Pasadena, California

Prepared for
Ames Research Center
under Grant NGL 05-002-229

National Aeronautics
and Space Administration

**Scientific and Technical
Information Office**

1978

TABLE OF CONTENTS

I. INTRODUCTION

Two investigations of separating turbulent flow have recently been carried out at GALCIT*, using a novel and relatively complex device called the flying hot wire. The first experiment is a study of flow past a stalled airfoil operating near maximum lift. This work is reported in detail by Wadcock in reference 1. The second experiment is a study of formation and shedding of vortices in the near wake of a circular cylinder. This work is reported in detail by Cantwell in reference 2. The present paper describes instrumentation which the two experiments have in common.

The basic problem with use of hot-wire anemometry in regions of high turbulence level is that the instantaneous flow may approach the probe from an awkward direction (for a recent appreciation of the problem, see reference 3 by Tutu and Chevray). A conventional X-wire array, having wires mounted at $\pm 45^{\circ}$ to the probe axis, will not have a unique response unless the relative flow direction is restricted to lie within this same range of $\pm 45^{\circ}$. The object of the flying-hot-wire technique is to increase the relative velocity component along the probe axis, and thus to decrease the relative flow angle, by mounting the probe on the end of a rotating arm.

Signals from a moving probe are statistically neither stationary nor homogeneous. High-speed data recording by digital means is therefore an integral part of the flying-hot-wire technique. In the case of the cylinder experiment, moreover, an important objective is to observe spatial and temporal phase relationships during the shedding process. This objective by itself would presumably require use of digital techniques even if the probe were stationary

---

*Graduate Aeronautical Laboratories, California Institute of Technology.

rather than moving. Finally, the highly nonlinear relationship between transducer signal (hot-wire voltage) and physical variable (vector velocity) makes data processing by computer a plausible element of experimental strategy from the outset.

Fifteen years of experience at GALCIT have established a number of hazards which accompany use of digital techniques, especially in graduate research. Digital systems are designed to record large quantities of data, often in a short time. Data acquisition should therefore not be made too easy, because of the temptation to substitute quantity for quality, and to fail to organize the measurements for relevance and accuracy. The temptation is particularly strong when working in a large and relatively expensive facility. It is also easy to become so absorbed in details of data handling as to lose touch with the real research problem. Perhaps the most serious hazard in practice is that a long time may elapse between an experimental attempt and a decision as to whether or not this attempt was successful. A poor first approximation in experimental technique may turn out to be also a poor last approximation. It is therefore essential that planning for the research should include adequate provision for the time and effort required for computer programming and preliminary data analysis. Moreover, this effort must be made in parallel with the actual experiment, not in series. Otherwise, the experimental results may never be completely assimilated or understood. We believe that these hazards were recognized and avoided to an acceptable degree in the present research.

II. THE FLYING HOT WIRE IN PRINCIPLE

2.1 Probe Self-calibration. -- One of the most attractive properties of the flying hot wire is the feature of self-calibration in pitch. As the arm

rotates in a uniform stream, the flow angle relative to an X-array varies over a wide range. Figure 1 shows a typical construction for the relative flow in laboratory coordinates. The angular displacement of the rotor arm, ϕ, is measured from top dead center and increases in the counter-clockwise direction. The relative flow angle, α, is zero when ϕ is zero and increases with increasing ϕ.

Two examples of the relative flow in rotating coordinates are shown in figures 2a and 2b after normalizing the magnitude of the three velocity vectors $\vec{u}_\infty$, $\vec{\omega}\times\vec{R}$, and $\vec{q}$ with u_∞. The uniform stream is now represented by the

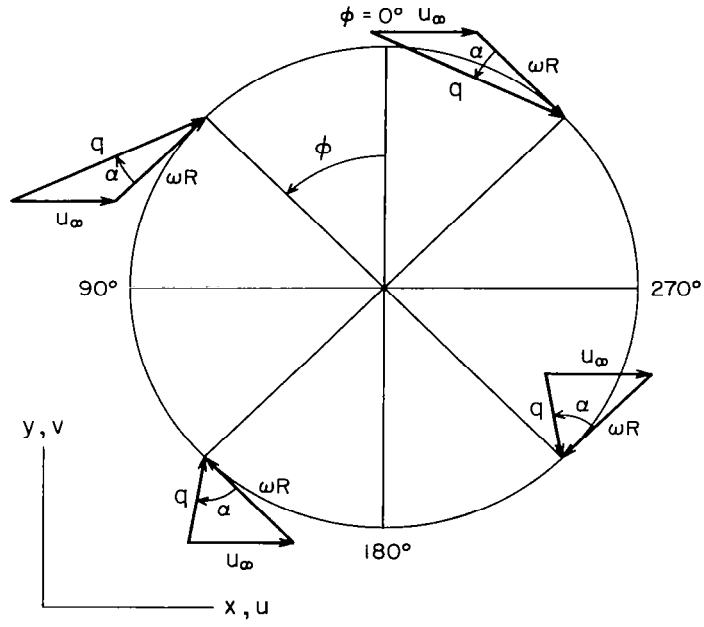

Figure 1. Flow relative to flying-hot-wire probe in laboratory coordinates. Uniform ambient flow is from left to right. Probe angular displacement ϕ is measured from top dead center and increases for counter-clockwise rotation. Relative flow angle α is measured from direction of probe motion to direction of relative velocity vector and is positive when relative flow is toward rotor hub.

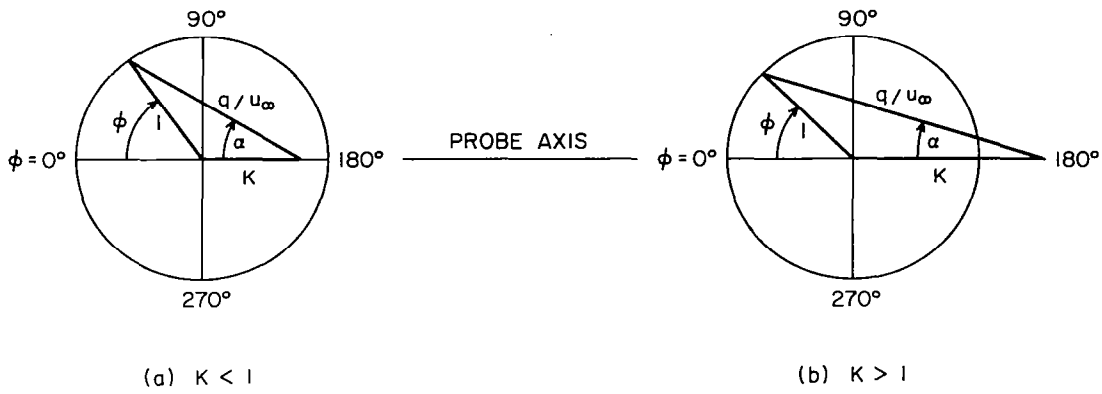

(a) K < 1 (b) K > 1

Figure 2. Flow relative to flying-hot-wire probe in probe coordinates. Angles are defined as in figure 1.
(a) Case of slow rotation, $\omega R < u_\infty$ or $K < 1$.
(b) Case of fast rotation, $\omega R > u_\infty$ or $K > 1$.

rotating unit vector. The parameter of the motion is evidently the ratio of rotor tip speed to stream speed, $K = \omega R/u_\infty$. Only positive values of K will be considered in what follows. For the case $K < 1$ (slow rotation, figure 2a) the angle α increases monotonically but non-uniformly with ϕ. For the case $K > 1$ (fast rotation, figure 2b) the angle α oscillates over a finite angular range less than $\pm 90^\circ$ as the rotor rotates at constant speed. From either figure, it follows that

$$\tan \alpha = \frac{\sin \phi}{\cos \phi + K} \qquad \left\{ \begin{array}{l} -90^\circ < \phi < 270^\circ \\ -180^\circ < \alpha < 180^\circ \end{array} \right\} \tag{1}$$

and that

$$\frac{q}{u_\infty} = (1 + 2K \cos \phi + K^2)^{1/2} \tag{2}$$

The relative motion is more conveniently expressed as a tangential component

$$U = q \cos \alpha \tag{3a}$$

and a radial component (taken positive inward along the radius, to be consistent

with the sign convention for α)

$$V = q \sin\alpha \tag{3b}$$

Finally, the transformation from flying to fixed coordinates is

$$u = (U - \omega R)\cos\phi + V \sin\phi \tag{4a}$$

$$v = (U - \omega R)\sin\phi - V \cos\phi \tag{4b}$$

where u and v are taken positive in the customary sense shown in figure 1.

Figure 3 summarizes the kinematic constraint imposed by equation (1) on the flying-hot-wire technique in uniform flow. Operation at fixed rotor speed corresponds to a horizontal traverse from left to right in the figure at constant $K = \omega R/u_\infty$. Although the angular displacement ϕ is most conveniently measured from top dead center for arm I, a revolution is considered to

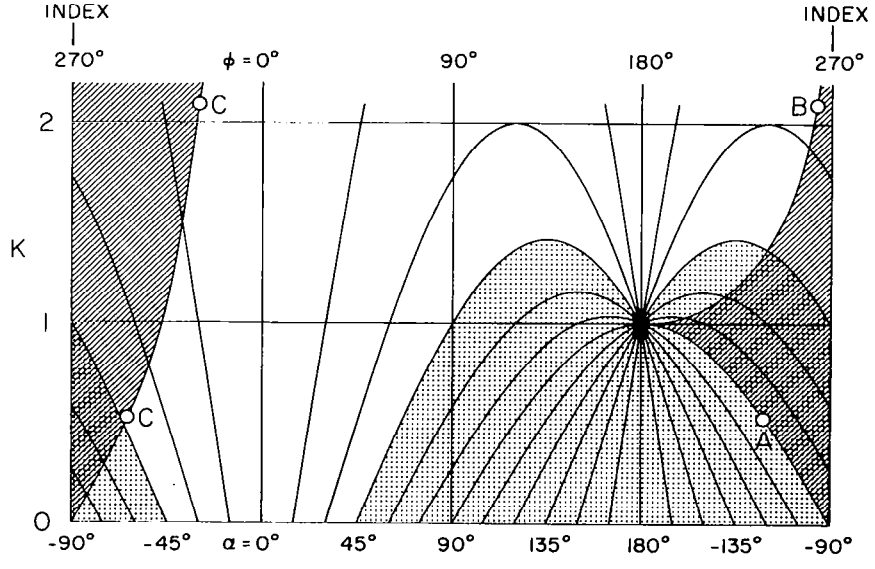

Figure 3. Operating constraints for ideal flying hot wire, defined for one full revolution. In slant-shaded region, probe is passing through wake of arm. In dot-shaded region, direction of relative flow is more than 45° from ideal probe axis. For points A, B, C, see figure 4.

begin when an index pulse occurs at the rear position $\phi = -90^{\circ}$ for arm I (see section 5.3 below). The lines of constant relative flow angle α are obtained from equation (1), neglecting any angular offset of the probe tip with respect to the rotor arm. Unless $K > \sqrt{2}$, the relative flow angle α will always fall outside the useful range $\alpha = \pm 45^{\circ}$ during some part of the revolution, as indicated by the dot-shaded region in the figure.

2.2 Wake Interference. -- The flying-hot-wire rotor and its supporting structure represent a potentially severe disturbance to the flow. One aspect of the problem is wake interference, which occurs when the probe passes through fluid which has previously come into contact with some part of one rotor arm or the other. Wake interference for two arms rotating in the same plane can be adequately treated by again neglecting any offset of the probe from the tip of the arm and by assuming that fluid in contact with the arm at any instant is thereafter convected uniformly downstream at the velocity of the free stream. The trajectory of the probe through the fluid is a cycloid, curtate if $K < 1$ and prolate if $K > 1$. Examples are sketched in figures 4a and 4b. Open circles refer to arm I and closed circles refer to arm II. The rotation cycle proceeds from right to left, toward negative values of x.

There is evidently no probe interference in the forward or upstream half of a revolution, since fluid touched in the range $0^{\circ} < \phi < 180^{\circ}$ is always convected away from the probe.

For $K < 1$, interference occurs in the range $180^{\circ} < \phi < 270^{\circ}$ (lower rear quadrant of a revolution) beginning at the point A in figure 4a, where the probe touches the envelope of arm positions and enters the wake currently being laid down by its own arm. A line tangent to the envelope defines both the instantaneous position of the arm and the instantaneous direction of motion of the point

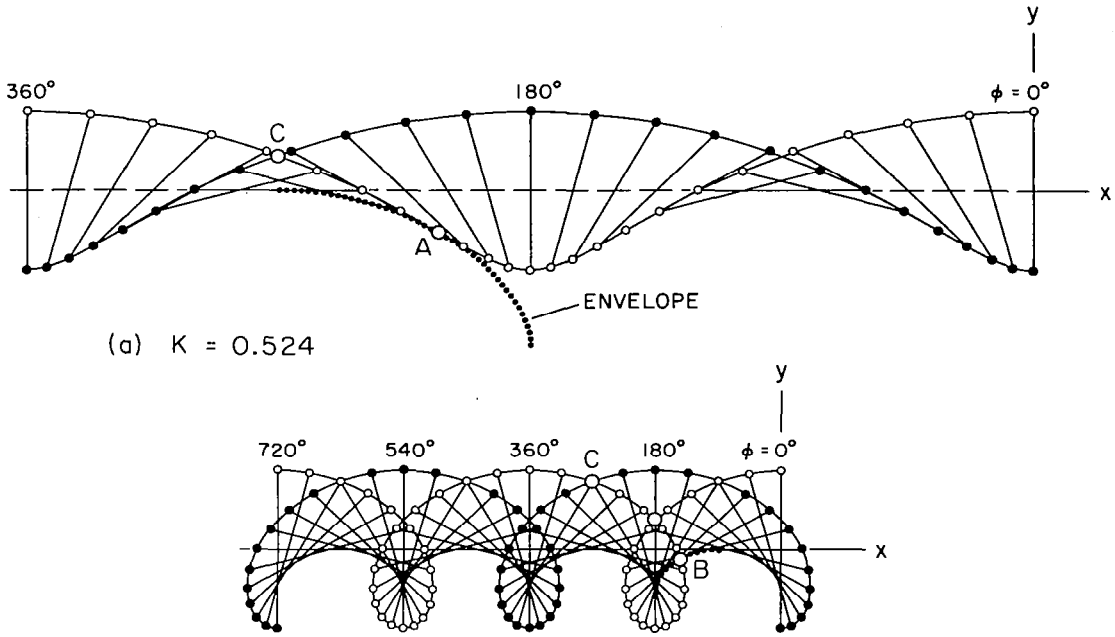

Figure 4. Geometric interpretation of probe interference. Successive positions of rotor arms are shown as viewed by observer moving with external stream. Time increases from right to left. Open and closed circles refer to probes on arm I and arm II respectively. At points A and B, probe I enters wake of arm I. At point C, probe I emerges from wake of arm II.
(a) Typical case of slow rotation, K = 0.524.
(b) Typical case of fast rotation, K = 2.094.

of tangency. Wake interference begins when the probe reaches this point of tangency at A, at which time the relative flow angle α at the probe is -90°. The interference boundary is therefore defined directly by equation (1),

$$K = -\cos\phi \qquad \left\{ \begin{array}{l} K < 1 \\ 180^{\circ} < \phi < 270^{\circ} \end{array} \right\} \tag{5}$$

For $K > 1$, interference occurs in the same range $180^{\circ} < \phi < 270^{\circ}$ (lower rear quadrant of a revolution) beginning at the point B in figure 4b,

where the probe enters the wake previously laid down as its own arm passed through the quadrant $90^\circ < \phi < 180^\circ$. At the position $\phi = 180^\circ$, for example, the outer part of the arm is obviously outrunning its own wake, because $\omega R > u_\infty$. However, the probe must eventually encounter the wake from the inner part of the arm. The equation of the envelope of successive arm positions is readily shown to be

$$x = \frac{u_\infty}{\omega} \sin\theta \cos\theta - \frac{u_\infty}{\omega} \theta \tag{6a}$$

$$y = -\frac{u_\infty}{\omega} \cos^2\theta \tag{6b}$$

where θ refers to past angular displacements of the arm. At any instant, the probe on arm I is at the position

$$x = -R \sin\phi - \frac{u_\infty}{\omega} \phi \tag{7a}$$

$$y = R \cos\phi \tag{7b}$$

where ϕ refers to the present angular displacement of the arm. On the interference boundary the coordinates x and y are equal. The boundary $K(\phi)$ is therefore defined by the parametric equations

$$-K \sin\phi - \phi = \sin\theta \cos\theta - \theta \tag{8a}$$

$$-K \cos\phi = \cos^2\theta \tag{8b}$$

$$\left\{ \begin{array}{l} K > 1 \\ 180^\circ < \phi < 270^\circ \\ 90^\circ < \theta < 180^\circ \end{array} \right\}$$

These equations may be solved numerically* to obtain the interference boundary for $K > 1$ shown at the upper right in figure 3.

The remaining and practically most important type of interference occurs in the range $270^\circ < \phi < 360^\circ$ (first quadrant of the upper half-revolution) beginning at $\phi = 270^\circ$ and ending at the point C in figure 4a or 4b, where the rearward arm passes out of the wake of the forward arm. In this case, the

*Note for the case $K < 1$ that the equations are satisfied by $\theta = \phi$ and $K = -\cos\phi$, as argued earlier on other grounds.

present position of the probe on arm I is given as before by equations (7). Past positions of the tip of arm II are given by

$$x = R \sin\theta - \frac{u_\infty}{\omega}\theta \tag{9a}$$

$$y = -R \cos\theta \tag{9b}$$

Coincidence in y requires $\theta = \pi - \phi + 2n\pi$, $n = 0, \pm 1, \pm 2, \ldots$ Coincidence in x and an obvious choice $n = 1$ then define the interference boundary

$$K = \frac{\frac{3\pi}{2} - \phi}{\sin\phi} \qquad \left\{ \begin{array}{l} \text{all } K \\ 270^\circ < \phi < 360^\circ \end{array} \right\} \tag{10}$$

shown at the left in figure 3.

The various regions where wake interference occurs according to this elementary model are slant-shaded in figure 3.

There is an interior boundary point between B and C in figure 4b which can be ignored if the two arms rotate in the same plane. A further kind of interference can occur if K is large enough ($K > 2.972\ldots$) so that the lower loops of the prolate cycloids in figure 4b intersect each other. However, such large values of K are outside the expected operating range of the flying hot wire, at least in a wind tunnel.

The message of figure 3 is now complete. Taking into account both wake interference and relative flow angle, probe calibration is best carried out at values of K less than 0.5. During data collection near $K = 1$, approximately the first quarter of the upper half revolution may be lost because of interference by the wake of the preceding arm. The figure also suggests several possible variations on the flying-hot-wire theme; angular offset in pitch for the probe axis (to displace the interference boundaries), lateral offset for the two arms (to avoid wake interference in the upper half revolution),

support of the rotor from the rear (to increase mobility in the tunnel test section), and so on. Finally, there is the obvious option of reversing the direction of rotation of the rotor to achieve lower relative velocities at the probe. None of these variations has so far been explored experimentally.

2.3 Operating Constraints. -- A variety of different and sometimes conflicting considerations govern the choice of model size, tunnel speed, and rotor tip speed for a particular experiment. Other things being equal, research in turbulence is potentially most productive when it is carried out at high Reynolds number. As a practical matter, other things are usually not equal. For example, the cylinder experiment is constrained to run at Reynolds numbers substantially below the critical value of about 350,000. For any experiment which involves detailed probing of a complex flow field, a large model is clearly desirable within whatever limits are imposed by unacceptable wall effects such as severe blockage or three-dimensionality of the mean flow. Since the fluctuation levels are high by definition, a ratio of rotor tip speed to tunnel speed of order unity is presumably necessary in order to minimize the probability that the instantaneous relative flow angle will be outside the useful range of $\pm 45^{o}$.

For a given data volume and a given value of K, advantages of high tunnel speed and high rotor speed include decreased testing time (and cost) and decreased drift in instrumentation. Disadvantages of high tunnel speed include increased chance of wire breakage, decreased hot-wire sensitivity, and increased dynamic loads and deflections for both model and probe. Disadvantages of high rotor speed include, in addition, increased rotor power, increased disturbance to the basic flow, increased self-interference from the wake of the rotor arms, and decreased time for on-line data processing.

Finally, calibration of hot wires for use in highly turbulent flow evidently requires a very large range of relative probe speeds. In particular, adjustment of hot-wire circuit parameters for good frequency response is best done at normal operating speed but in steady relative flow. Hence, either the probe should be capable of rotating in still air at roughly twice the normal rate, or, if the probe is held fixed, the tunnel should be capable of running at twice the normal speed (four times the normal dynamic pressure). For the main body of a dynamic calibration, on the other hand, figure 3 shows that a relatively small ratio of rotor tip speed to tunnel speed is desirable in order to move the active pitch-angle range toward the top of the rotor arc and thus minimize contamination of calibration data by the wake of the preceding rotor arm.

III. THE FLYING HOT WIRE IN PRACTICE

3.1 Mechanical Details. -- Figure 5 is an assembly drawing of the flying-hot-wire apparatus as it emerged from a lengthly design and development process. The actual tunnel installation is shown in figures 6 and 7, which are photographs taken in the tunnel test section during the cylinder and airfoil experiments respectively. The rotor arms are fabricated of elliptical stainless steel tubing having a chord of 3.27 cm and a thickness/chord ratio of about 0.32. The arms are attached to a hub which is mounted on the shaft of a printed-circuit DC motor. The motor case is itself clamped in a recess at one end of a 200-cm vertical strut of 5-cm by 20-cm rectangular steel tubing. The other end of the strut is bolted to a vertical slide assembly which rides on the saddle of a lathe bed below the wind tunnel. The vertical traverse has a

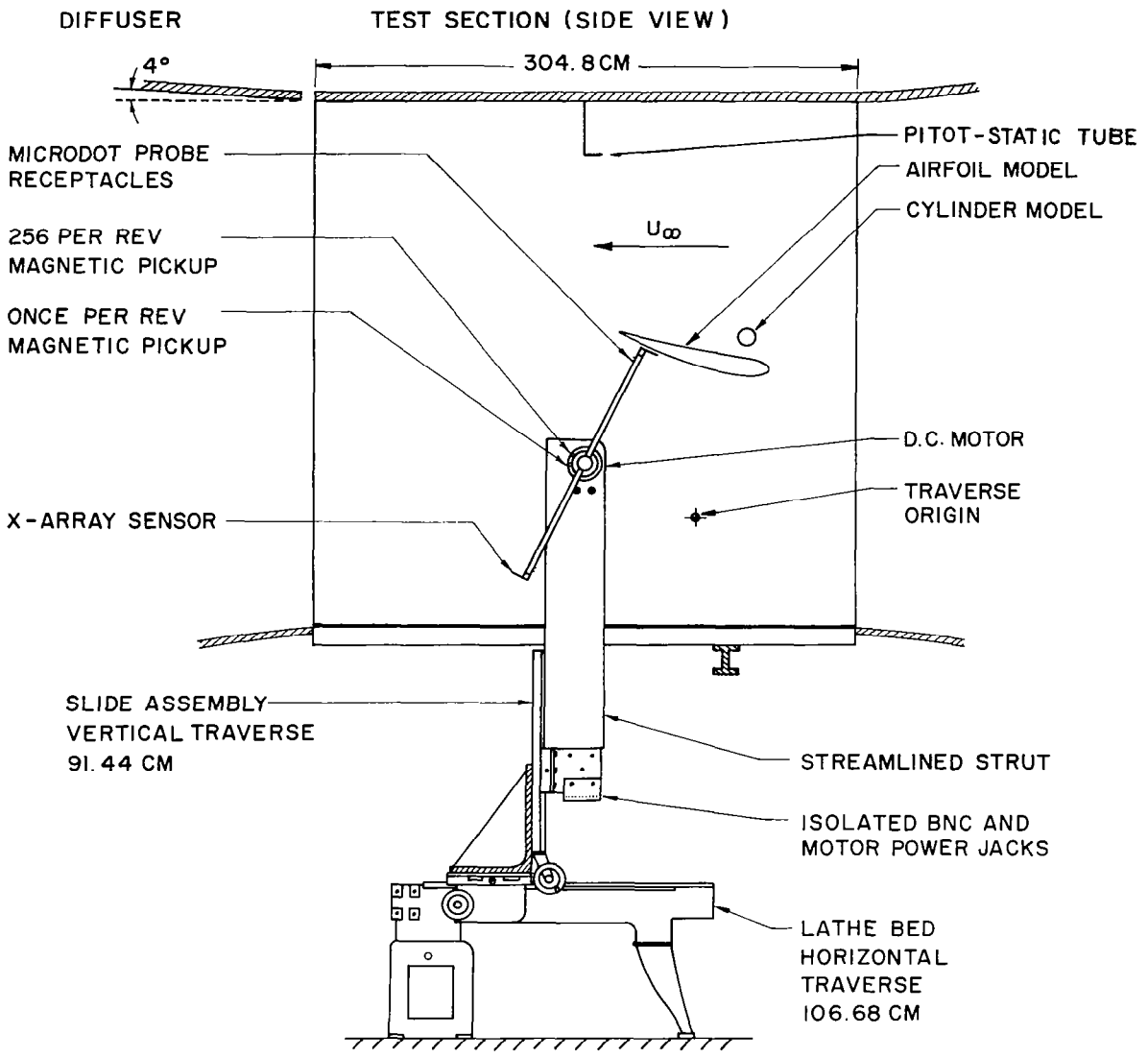

Figure 5. Installation of flying-hot-wire apparatus and traverse in test section of GALCIT 10-foot wind tunnel. In side view,

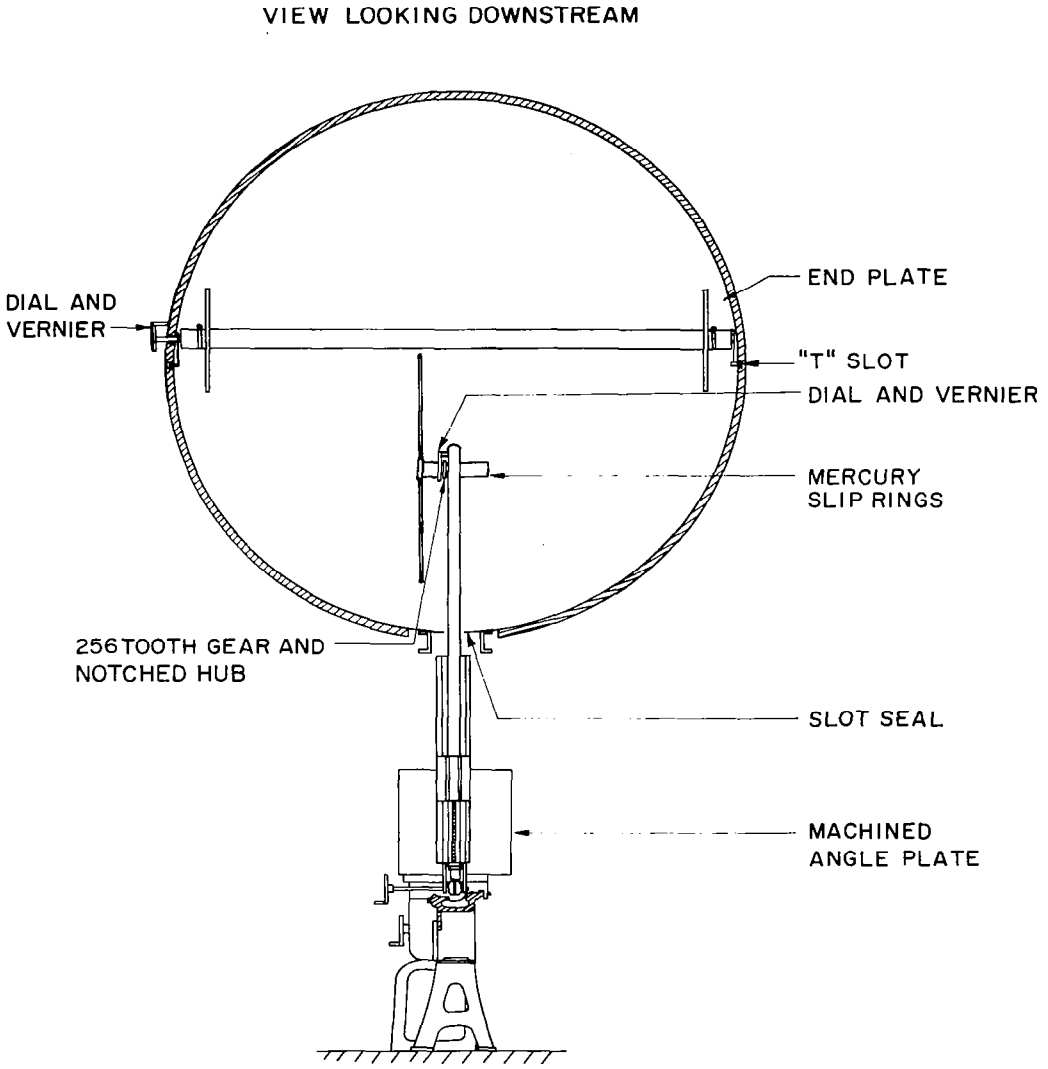

flow is from right to left and rotor rotates clockwise. In view looking downstream, airfoil model is omitted for clarity.

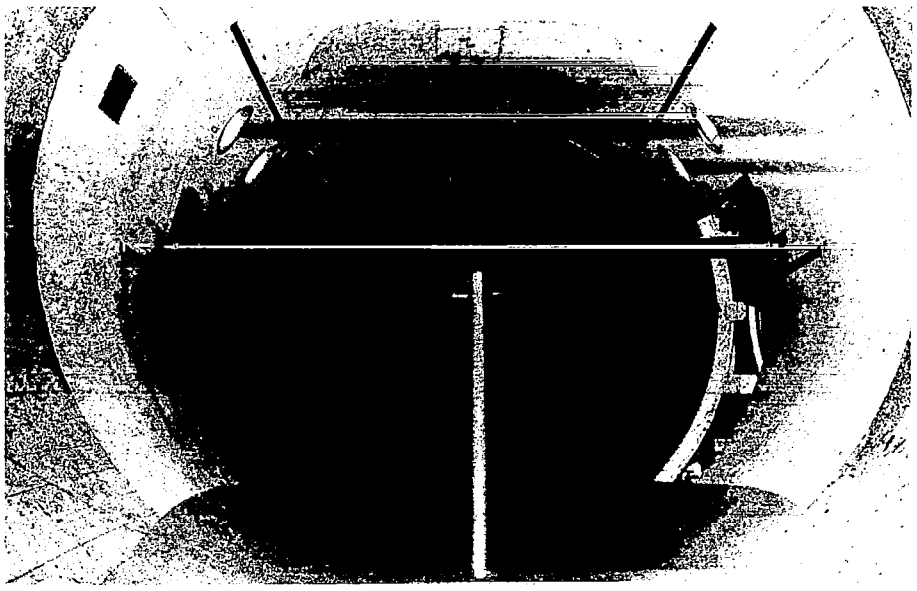

Figure 6. Photograph of cylinder model and flying-hot-wire apparatus in GALCIT 10-foot wind tunnel. View looking downstream, showing strut and rotor near maximum elevation.

range of 36 inches* and is repeatable to 0.001 inch. The horizontal traverse has a range of about 110 cm and is repeatable to about 0.01 cm. The part of the rectangular strut which is exposed to the airflow is streamlined by wooden cladding shaped to a NACA 0024 profile section. The rotor arms, however, are not streamlined. The (unproven) assumption is that use of a moderately high-drag section undoubtedly imposes a penalty in terms of disturbance to the flow and in terms of rotor power, but that this penalty is more than offset by the advantage of reduced lateral bending forces on a low-lift section in regions of large-scale lateral turbulence. In fact, a shaft extension was added to increase the distance between the motor case and the rotor after a preliminary

*The slide assembly is designed in the English system; vertical dimensions and displacements are therefore usually given in inches for the sake of accuracy.

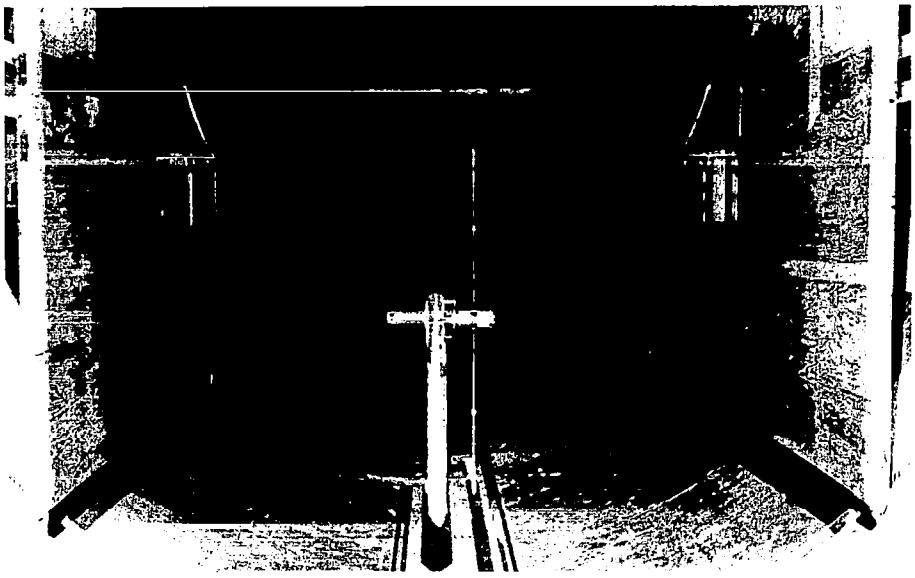

Figure 7. Photograph of airfoil model, false walls, and flying-hot-wire apparatus in GALCIT 10-foot wind tunnel. View looking upstream. Note added brace wires on rotor, not present in figure 6.

test in the tunnel showed that severe lateral arm vibration could be excited at certain speeds by the double impulse received as the retreating arm passed through the flow field around the streamlined strut. Between the cylinder experiment in late 1974 and the airfoil experiment in early 1975, the arms were also stiffened by addition of light brace wires running from the hub to about the midpoint of each arm (cf. figures 6 and 7).

The test section of the wind tunnel has a narrow full-length slot at the bottom which allows traversing in the streamwise direction. For the cylinder experiment, this slot was sealed by plywood and tape except for a small clearance gap around the streamlined strut. As a matter of convenience, therefore, most of the measurements in the cylinder wake were made by

traversing vertically at three streamwise locations. For the airfoil experiment, the slot was sealed by a cloth strip with two central zippers running upstream and downstream from the strut; the traverse mechanism could then be moved freely in both the vertical and the horizontal direction.

The diameter of the rotor is about 150 cm. Choice of diameter was governed by a desire to minimize the influence of the supporting structure on the flow around the test model, and also by considerations of rotor inertia, rotation rate, sampling scale and frequency, and aerodynamic torque. The diameter finally chosen is the largest which is compatible with the size of the GALCIT wind tunnel (cylindrical test section 10 feet in diameter) without foreclosing the possibility of traversing past the model while the tunnel is running.

3.2 Phase-lock Servo. -- The aerodynamic part of the torque on the rotor consists of a steady component which is roughly proportional to $(\omega R)^2$ and a periodic component (at twice the rotor frequency) which is roughly proportional to u_∞^2. The ratio of the two torque components (but not their magnitude) is essentially fixed by the value of the operating parameter $K = \omega R/u_\infty$. For values of K near unity and for values of u_∞ near 30 m/sec, a reasonable estimate of the periodic component of torque is one meter-newton. The need to maintain closely constant speed in spite of large variations in torque was met by development of a phase-lock servo drive. In essence, a phase-lock servo is a phase-lock loop in which the voltage-controlled oscillator is replaced by an encoder driven by a DC motor. The motor acts as a mechanical low-pass filter whose time constant is determined by the inertial load. Phase-lock servos are normally used to control light loads such as tape drives, and the large inertia of the flying hot wire introduces some special problems both from the standpoint of stability and from the standpoint of power required for precise

control of a considerable mass.

One design condition for the phase-lock servo was that it should be operable by a single control. That is, it should lock reliably at any desired speed, and it should execute smoothly any desired speed change, without adjustment of the loop parameters. To meet this condition, and also to circumvent the possibility that the loop might lock to a harmonic of the input frequency, the error signal from the phase detector is reinforced by a signal proportional to the error in frequency. Lock is achieved only when both errors are driven to zero.

Strictly speaking, a phase-lock servo is not a velocity servo, but a position servo. The angular position of the DC motor is encoded by a 256-tooth precision gear and a magnetic pickup. The pickup provides a clean square-wave TTL output at 256 pulses per revolution which serves as feedback input to the phase detector. The other input to the phase detector originates in a preset counter (in the data-acquisition system) as a 200-kHz crystal-controlled pulse train. A series of decade up/down counters divides the 200-kHz frequency by any desired decimal integer from 1 to 999 as selected on thumbwheel switches. The phase detector compares the divided signal to the pulse train from the encoder on the motor shaft, and produces an error signal proportional to the phase difference between the two. In the out-of-lock condition this error signal also contains a component proportional to the frequency difference.

The error signal is input to an analog integrator which in turn controls a bipolar power amplifier capable of providing 20 amperes at 50 volts to the motor driving the flying arm.

Since loop gain must be kept high to maintain strong locking characteristics, and since the inertial load of the rotor is large (14 newton-cm-sec),

the motor-rotor combination contributes nearly 90^{o} of phase lag at the unity-gain crossover frequency of the open-loop transfer function. As a result the loop contains three integrations and is inherently unstable. To achieve stability, a lead-lag compensation network is introduced between the phase detector and the analog integrator, and a resistor is placed in series with the capacitor in the feedback path of the integrator. The effect of these two adjustments is to give the open-loop transfer function a stable phase margin of 36^{o} at the unity-gain crossover frequency.

A phase-lock servo controlling a large inertial load treats the DC motor rather harshly. The control signal to the motor has an AC component which is a large-amplitude sawtooth, constantly pushing the motor hard on and hard off to control the position of the arms. The mass of the arms effectively filters this AC component, so that no undue motion occurs at the tip. However, under certain operating conditions a resonance condition apparently occurs, as indicated by a high-pitched whine from the motor. This resonance has an observable adverse effect on the hot-wire signals, either because of mechanical motion of the wires (there was occasional wire breakage when operating near or passing through the resonance) or perhaps because of electrical noise induced in the hot-wire circuits by the resonating motor armature. The problem is not serious once it is recognized, because the rather narrow-band resonance condition (encoder frequency 860 Hz ±50 Hz) is easily avoided.

In the locked condition the average speed of the rotor is as constant as the frequency of the crystal oscillator. The instantaneous speed varies about one cm/sec twice per revolution due to the large torque perturbations from the flow. The excellent performance of the servo system is due in part to the fact that the printed-circuit motor has low inductance (because of the absence

of iron in the armature) and is essentially free of cogging. A second useful property of the motor is the pancake shape, which is well adapted to fit in the strut used to support the rotor.

3.3 Electrical Details. -- A hot-wire probe is mounted in a clamp holder at the end of each arm. A square section on the probe body mates with a square recess broached in the forward end of the clamp, allowing the probe to be rotated in increments of 90° without losing registration.

Hot-wire signals are carried via microdot cables through the hollow rotor arms to the hub and thence through the hollow motor shaft. A short section of the microdot cables exposed to the airflow near the rotor tip is normally protected by stiff tape. If the tape is not applied with care, buffeting and vibration can impair the performance of the servo rotor drive. Electrical connections from rotating terminals to stationary terminals are made through a set of twelve slip rings. The rotor was first equipped with silver-graphite rings. However, the observed resistance fluctuations (about 10 milliohms rms, well above the manufacturer's specification) were too large to be tolerated within the active bridge arm. The silver-graphite slip rings were therefore replaced by mercury slip rings which have much smaller resistance variations. Eight rings are required for two hot-wire probes (there are no common leads). The remaining four rings carry power, ground, and signal connections to an optical proximity sensor located on the end of arm I.

Finally, microdot cables carry the various signals through the inside of the streamlined strut to isolated BNC connectors below the wind tunnel. The relatively long cables contribute altogether about 25 percent of the total resistance in the active arm of the hot-wire resistance bridge. Adequate compensation for cable inductance is available in the hot-wire circuitry.

Among other uses, the optical proximity sensor mounted on arm I of the rotor serves to establish the angular position of successive data samples along the probe arc. The sensor contains a light source and a detector whose outward lines of sight intersect about 0.6 cm from the sensor body. The response time of the detector is a few microseconds. By placing a narrow reflective target at approximately the same elevation as the rotor axis and at a suitable radius, a sharp voltage pulse can be observed once per revolution as arm I passes the target. The wave form of this pulse can also be observed statically by clamping the rotor arms in a horizontal position and traversing vertically past the target. In particular, the traverse can be stopped on some convenient point of the wave form, and the voltage noted. When the rotor is set in motion, occurrence of this same voltage means that the arms are passing through the horizontal position. The elapsed time from this position to the first data burst after the index pulse (see section 5.3 below) is readily measured and converted to angular displacement using the known rotor speed.

3.4 Operating Envelope. -- After fabrication of the rotor, supporting structure, and phase-lock drive, a preliminary test was carried out in the tunnel to check for satisfactory operation. Except for the increase in motor shaft length already mentioned, no substantial changes were required. The spatial resolution and data rate based on 256 samples per revolution were acceptable. The one remaining weakness of the design is a slight lack of rigidity in the streamwise direction at the saddle of the vertical traverse. At the highest attainable dynamic pressure and at the upper limit of vertical travel, fluctuating air loads on the streamlined strut and rotor hub can cause streamwise vibrations at the hub as large as 0.5 cm at frequencies near 10 Hz. This behavior was considered when choosing tunnel speed and when providing

sufficient clearance to avoid striking the model.

In practice, the speed range available for the flying-hot-wire rotor in still air is from about 50 rpm to about 700 rpm (tip speeds from 3.7 m/sec to 53 m/sec). The lower limit is determined mainly by dropouts in the encoder pulse train when the gear teeth pass the magnetic pickup too slowly.* The upper limit is determined mainly by the power available from the servo drive system. This still-air range is shortened, particularly at the upper end, when the tunnel is running, because the servo power amplifier is unable to maintain lock when both torque and torque fluctuation are large. As a precaution, it is normal practice to monitor the presence of lock continuously by observing an oscilloscope display of the unfiltered output of the phase-detector circuit.

The operating range of the GALCIT 10-foot wind tunnel is fixed by the blade setting for the tunnel fan, a setting which is not readily changed. The blade setting is best chosen so that the upper limit for tunnel speed lies only slightly above the speed desired for the experiment. This choice maximizes the range available for hot-wire calibration between the test condition and the practical lower tunnel limit established by speed regulation of the DC fan motor at low load. Given stable tunnel operation in the range (say) from 5 m/sec to 40 m/sec, the smallest relative velocity available at the probe is about 9 m/sec, none too small a value in practice. For a given blade setting, the effect of this restriction is evidently to influence the decision as to model Reynolds number toward a high value within the fixed operating limits of the tunnel.

During one test early in the research (cylinder experiment, tape 9) the rotor was operated over a wide range of rotor and tunnel speeds in the empty

*Use of an optical encoder rather than a magnetic one would obviate this problem, at the cost of a substantial increase in the complexity of the rotor hub design.

test section. The main objective at the time was development of data-acquisition programs, and the data have no permanent value. However, the raw data do serve to confirm experimentally the position of the hypothetical wake interference boundary in figure 3. The real flying-hot-wire device differs in several respects from the ideal device of figure 3. For one thing, the probe tip is offset so that it leads the arm by several degrees. For another, the effective chord of the arm is increased near the tip by the presence of external cables running from the probe to the arm. The experimental interference boundary, shown in figure 8, does not seem to be much affected. Inspection of the raw data also indicates that the rms voltage fluctuation in the wake interference region is typically no more than two or three times larger than the value in the free stream (cf. the oscilloscope trace in figure 9 below). Calibration

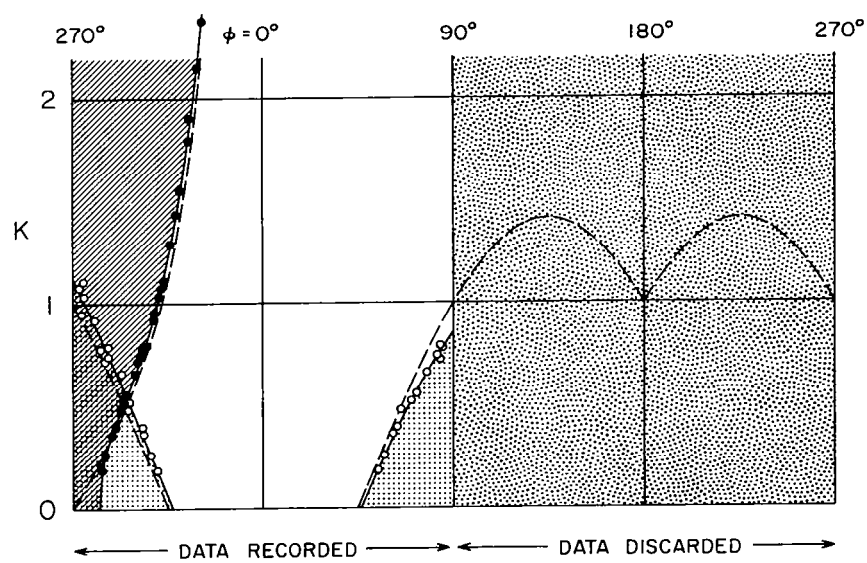

Figure 8. Experimental wake-interference boundary (solid points) and maximum-flow-angle boundary (open points) compared to ideal boundaries (dashed lines). Angle ϕ is arm position defined as in figure 3, without regard to probe offset or timing of INDEX pulse.

data obtained in the interference region are therefore not necessarily contaminated beyond use.

Figure 8 also shows the observed boundaries for a relative flow angle at the probe of $\pm 45^{\circ}$, as evidenced by a shallow (and hence slightly ragged) minimum in the voltage signal from one or the other wire of the X-array. The deviation of the real boundary from the ideal one is consistent with an effective rotation of the X-array through the offset angle of 5.64° by which the probe tip leads the rotor arm (see figure 14b below).

IV. RELATED INSTRUMENTATION

4.1 Solo System. -- The central element in the flying-hot-wire instrumentation is a computer-controlled data-acquisition system. The analog-to-digital converter (ADC) has a resolution of 14 bits plus sign and is capable of an overall conversion rate as high as 400,000 words per second while multiplexing as many as 16 channels. The computer has 32K 16-bit words of core memory. Peripherals include phase-encoded magnetic tape transport, cartridge disc, plotter, high-speed paper tape reader, and teletype.

The main data system is contained in a double-bay rack which is mounted on an air-cushion pallet so that it can readily be moved from one experimental site to another. The system weight of about 400 kg is carried by six air bearings which are pressurized by a vacuum-cleaner blower equipped with suitable speed control.

Although the computer and its peripherals constitute a powerful disc operating system, in an experimental context the system is often treated simply as a cosmic voltmeter. An important property of the data system is that it is designed and intended to be operated and managed entirely by the person

running the experiment. To encourage this view, the system is referred to as the "Solo System". During its first two years of operation the system has served as many as four experiments concurrently, moving from one site to another as often as twice a week.

4.2 Hot-wire Anemometers. -- Several channels of constant-temperature anemometry were constructed particularly for these experiments.* The circuit design follows a design recommended by Perry and Morrison in reference 4, with minor changes to accommodate low-drift, fast-response IC amplifiers. Design and fabrication were supervised by Dr. Perry, who was associated with this research during a study leave at CIT. He also carried out computer simulations to predict the response of the circuit to large signal inputs, such as might be encountered by the flying hot wire when traversing the near wake of the cylinder model. The results indicate that a square-wave test for this circuit will reproduce quite well the system response to be expected from application of a square wave of velocity. The results also indicate that, for large velocity fluctuations, frequency interactions can contribute some error in measurement of $\overline{u'v'}$ correlations. This fact influenced the choice of rotor speed for the wake measurements and threw its weight on the side of lower speeds.

4.3 Intermittency Meter. -- Intermittency is an idealized property of turbulent flows, and its measurement therefore tends to be a partially subjective process. The conventional definition assumes that the motion at any point in the flow at any instant can be classified as either turbulent or non-turbulent. In particular, it is common practice to call the motion turbulent if there is

*The anemometer design and operation are described in an internal CIT memorandum, "Manual for Matilda Meter Constant Temperature Anemometers", GALCIT, October 1975, by B. Cantwell.

appreciable energy at high frequencies. This practice is quite at odds with the spirit of the present research, in which the concept of spectrum plays no substantial role. Moreover, the normal sampling frequency is by far too low to include the frequencies involved in intermittency. As a matter of convenience, therefore, the classification process was carried out by analog methods in real time.

Continuous analog signals from both wires of one X-array are first separately differentiated, to emphasize high frequencies, and then added. The combined signal is band-pass filtered and rectified and fed into a comparator with an adjustable threshold level. The output of the comparator is an irregular pulse train corresponding to portions of the input signal above the threshold level. Each time the flying hot wire passes through turbulent fluid, a burst of such pulses is produced. This burst is fed to a retriggerable one-shot whose output remains high whenever the time interval between input pulses is less than the pulse width of the one-shot. The output of the intermittency circuit is a TTL-compatible digital signal which is continuously available to the data system and is recorded as the least significant bit of each data sample.*

Figures 9 and 10 show two examples of analog input signal and digital output signal for the intermittency circuit. In the lower trace of each figure the filtered but unrectified composite analog signal has been added electronically to the digital intermittency signal, to show the quality of the discrimination technique. In figure 9, the relatively weak noise in the early part of the hot-wire signal is associated with the passage of the probe through the turbulent wake of the preceding rotor arm (see section 2.2 above and especially figure 3).

*The 15 bits from the ADC are left-justified in the 16-bit computer word, leaving the least significant bit free for this or other use.

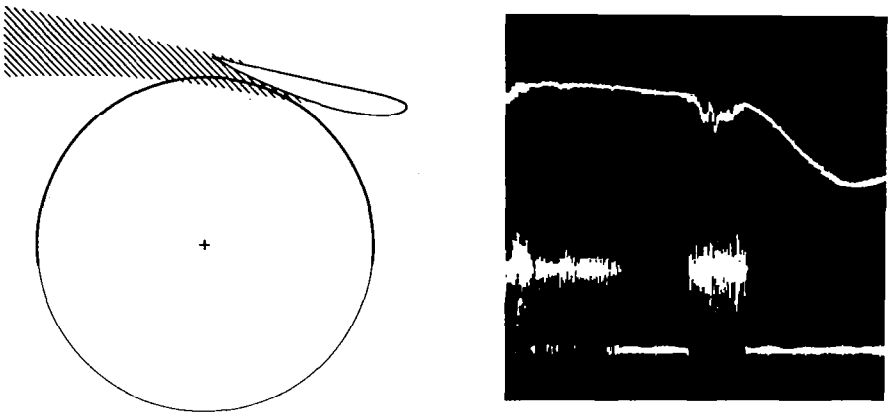

Figure 9. Example of intermittency signal for airfoil experiment (tape 16, file 12). Display includes raw signal from one wire during upper half revolution. Oscilloscope is triggered by INDEX pulse. Filter passband is 1.0 kHz - 6.3 kHz. One-shot pulse width is 0.4 msec.

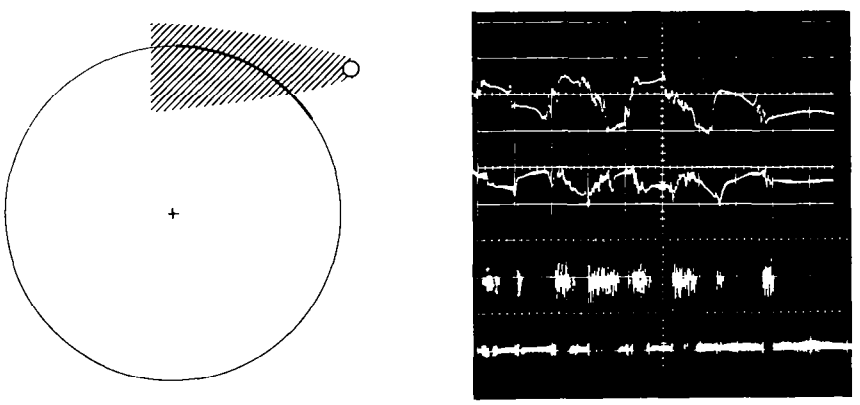

Figure 10. Example of intermittency signal for cylinder experiment (tape 25). Display includes raw signal from both wires of one X-array during part of upper half revolution. Oscilloscope is triggered by INDEX pulse but uses expanded sweep (5x). Filter passband is 1.0 kHz - 6.5 kHz. One-shot pulse width is 0.7 msec.

The subsequent passage of the probe through the airfoil boundary layer can be identified by the dominance of energy at larger scales.

Oscilloscope displays like those in figures 9 and 10 are useful in adjusting the threshold level so as to avoid triggering on noise in laminar regions, and in adjusting the one-shot pulse width so as to avoid indication of laminar flow in regions which are thought to be turbulent. The pass band of the filter, once set for satisfactory operation, is normally left fixed unless the rotor tip speed is changed (to zero, for example). The operation of the intermittency circuit was found to be little affected by changes in filter pass band, at least up to an upper cutoff of 20 kHz, indicating that the hot-wire signals contained useful information up to this frequency.

No systematic study was made of the effect of variations in threshold level or in one-shot pulse width on indicated intermittency. Only one intermittency circuit was used (although several were available), and no attempt was made to commutate the analog input signals or the digital output signal during alternate half revolutions of the flying arm. The signals used were always from the wires designated L-0, L-1 (i.e., "last channel minus zero", "last channel minus one"), and are valid for the first half of each revolution only.

The intermittency circuit described here is subject to a difficulty which is common to most such circuits. There is a slight lag in response on leaving a turbulent region, as shown for a typical signal in figure 11. In the present instance the lag occurs because the retriggerable one-shot remains on for a time equal to its preset pulse width (normally about 0.5 msec, or about half the sampling interval). The flying-hot-wire technique has another quite useful self-correcting property in this situation. Because the probe is moving, so that the mean intermittency data are dynamic rather than static, a plausible

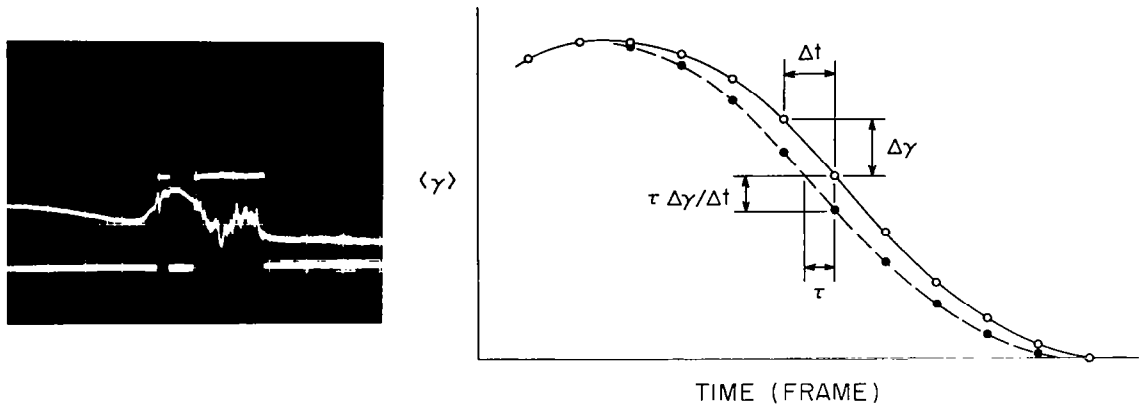

Figure 11. Typical oscilloscope trace showing raw hot-wire signal and associated intermittency signal with exit lag. Display is chopped single-beam. Sweep rate is about 3 msec/cm. Method used to correct mean intermittency data for exit lag is indicated in sketch at right.

a posteriori correction can be made to remove the lag. Denote the sampling interval by Δt and the preset pulse width of the one-shot by τ. Typical uncorrected mean intermittency data along a probe trajectory might appear as shown by the open points and the solid line in the sketch at the right in figure 11. After a displacement backward in time by an amount τ in regions of decreasing $\langle\gamma\rangle$, the same data appear as shown by the dashed line. Now at each data station the intermittency circuit indicates turbulent flow for a fraction $\langle\gamma\rangle$ of the data samples. Whenever the intermittency is decreasing, the net rate of interface crossings from turbulent to laminar flow per unit time is $-\Delta\gamma/\Delta t$. The number of such crossings in the time interval τ is $-\tau\Delta\gamma/\Delta t$. This is the number to be subtracted from $\langle\gamma\rangle$. It is also the vertical distance between the original (solid) and displaced (dashed) curves in the sketch. The correction thus amounts simply to displacement of the original time coordinate t backward in time by an amount τ, followed by displacement of the original $\langle\gamma\rangle$

downward to the new curve as shown by the solid points in the sketch.

V. DATA ACQUISITION

5.1 Programming. -- The Solo System is a fully implemented disc operating system which can be programmed in several commonly used high-level languages (FORTRAN, ALGOL, BASIC). However, because of massive data-handling requirements associated with the flying-hot-wire technique, especially the need for efficiency and economy in the use of available core memory, data acquisition and editing in the present experiments are carried out using stand-alone programs written in assembly language. These programs make no use of the operating system.

There are five main data-acquisition programs. The original program, MSTRY, was designed mainly for hot-wire calibration. This program assumes that two X-wire probes are present on the rotating arm. During each half-revolution, two channels of data are recorded from the probe which is currently advancing into the stream. The second program, NOMO, is similar except that rotation is simulated rather than real. The third program, PRESS, is like NOMO except that it records one pair of data channels continuously rather than two pairs alternately. The fourth program, RAMP, is a major modification of MSTRY designed particularly for the cylinder vortex-shedding measurements. Several data registers are reduced in size to suit the 16K words of core storage which were available at the time of the cylinder experiment. Two shedding-phase signals also receive special treatment. The fifth program, STALL, is also a modification of MSTRY. It is designed for 32K words of core storage, but some editing operations are deleted to accommodate the higher probe speeds used in the airfoil experiment.

Management of data acquisition is similar in all five programs. Before each run (i.e., each file), several octal parameters are entered manually into consecutive memory locations:

ID	File identification number	
NREV	Number of revolutions	
NREC	Number of tape records	
NCHAN	Number of analog channels	
NSKIP	Number of frames to be skipped	RAMP only
NSAVE	Number of frames to be saved	RAMP only

Starting the computer then causes several standard operations to be carried out. A gap is written on the magnetic tape. The multiplexer is initialized to last channel. The first direct-memory-access (DMA) transfer from the ADC to core memory is set up but not started. Several status checks are made, whose nature is more or less self-evident from a list of octal codes inserted in the program for display on the computer front panel in the event that a run is stopped by a programmed halt:

102021	NREV/NREC not an integer	before run
102022	ADC switches not in "normal"	before run
102023	ADC does not respond	before run
102024	Cannot find "last channel"	before run
102025	Tape transport not on line	before run
102026	No write ring in tape reel	before run
102027	Editing takes too much time	during run
102030	124 bad revolutions	during run

Having prepared itself for data acquisition, the system remains in a state of suspended animation until a control line called RUN is set true (see section 5.3 below).

5.2 Timing and Control. -- In normal operation, data acquisition is automatic, under joint control of data logic circuitry in the flying-arm

controller, control logic circuitry in the ADC, and DMA circuitry in the computer*. No program supervision is necessary except for verification, at the end of each revolution, that the data have the correct format and are properly synchronized. During the remaining time the computer is free to edit and dispose of data obtained during earlier revolutions.

The fundamental time base for the experiment originates in a magnetic pickup and a 256-tooth gear on the rotor shaft. The output of the magnetic pickup is a square-wave ENCODER signal which serves two important purposes. The first is to provide the feedback signal required by the phase-lock system which drives the flying arm at constant speed (see section 3.2 above). The second is to control the timing, and hence the position in the flow, of the hot-wire measurements. The circular trajectory traced out by the hot wires has a nominal diameter of 151.2 cm and a circumference of 475.0 cm. Specification of a 256-tooth gear then implies that digital data will be obtained every 1.86 cm along the arc. This spacing was accepted as adequate for boundary-layer work or for resolving the shape and structure of free vortices having a size comparable to or larger than the cylinder diameter of about 10 cm.

The data logic in the flying-arm controller is shown schematically in figure 12. It includes four binary-coded toggle switches which specify the number N of analog channels to be sampled in a burst mode as each gear tooth passes the magnetic pickup. A countdown channel counter is repeatedly preset to this value N at each negative transition of the ENCODER signal. At the next

---

*ADC operation is described in the Preston manual "Preston GM Series Analog-to-Digital Conversion Systems". DMA operation is described in the Hewlett-Packard manual "A Pocket Guide to the 2100 Computer". The hardware and software interfaces between the ADC and the computer are described in an internal CIT memorandum, "Notes on ADC Operation", Solo System Memo No. 2, May 1974, by D. Coles.

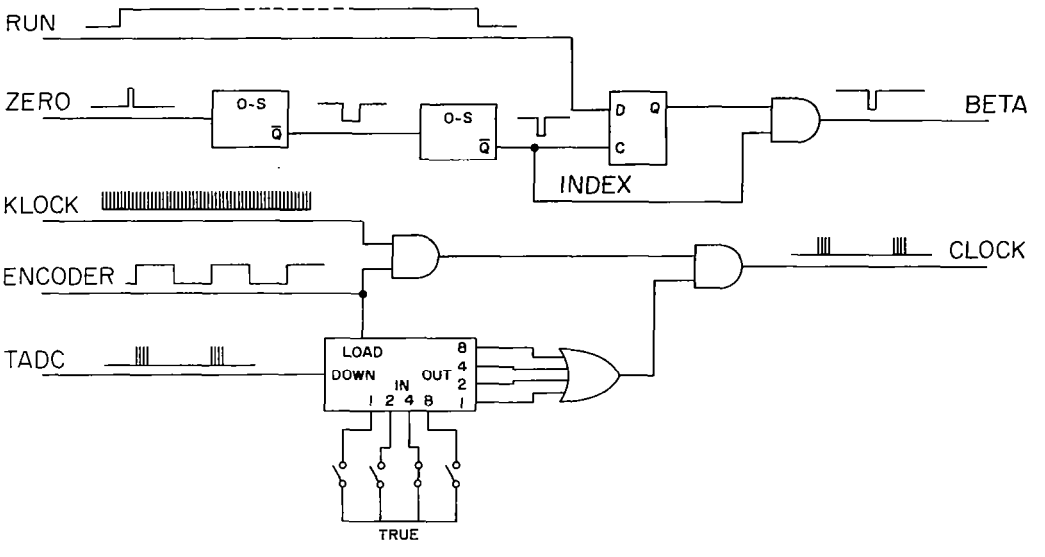

Figure 12. Schematic diagram of flying-arm controller.

positive transition, KLOCK pulses from a 200-kHz clock oscillator are gated to the ADC as CLOCK pulses. Each CLOCK pulse initially causes the multiplexer to switch to the next channel. After a short pause for signal settling in the sample-and-hold circuitry (settling time 1.5 μsec), a pulse called TADC (trigger ADC) is generated internally in the ADC to hold the input voltage and to begin a conversion (conversion time 1.7 μsec). The TADC pulse is transmitted to the channel counter, which counts down from N toward zero. The reason for counting TADC pulses rather than CLOCK pulses is that the KLOCK and ENCODER pulse trains are essentially asynchronous (although both are derived from the same crystal time base) on the time scale of the 175-nsec pulse width of KLOCK. Counting of TADC pulses guarantees that the ADC has recognized and responded to a CLOCK pulse by making a conversion, and hence avoids the problem of partial CLOCK pulses. When each conversion is complete, an end-of-conversion (EOC) pulse from the ADC notifies the DMA

channel that a new word is ready for transfer to core memory. After N channels have been converted, the zero state of the channel counter in figure 12 inhibits further CLOCK pulses to the ADC. In this manner a burst or frame of N words, spaced at invervals of 5 μsec, is acquired each time a gear tooth passes the magnetic pickup.

The number of channels, N, appears explicitly in two other places in the system. Another set of binary-coded toggle switches on the ADC front panel is used to select N consecutive channels (out of 16 channels available) by specifying the first and last channels. The multiplexer advances from one channel to the next, modulo 16, last channel being followed by first channel. The number N = NCHAN also appears in the program, where it is used to set up each DMA transfer as a block of 256 x N words of data. With N = 12, for example, a DMA transfer involves 3K = 3072 words of data for each revolution of the flying arm. Any discrepancy among these three specifications of the number N tends to cause format or synchronization errors such that a run will be automatically aborted after about 100 revolutions.

5.3 Self-synchronization. -- A second magnetic pickup and a notched ring on the rotor shaft are used to generate a single ZERO pulse once per revolution, at a time when the rotor arm is approximately horizontal (see figure 12). The timing of a delayed version of the ZERO pulse, called INDEX, can be varied electronically over a small range with respect to adjacent ENCODER pulses, so that the INDEX pulse occurs roughly midway between data bursts. A typical arrangement is shown in figure 13. The timing of the four events labelled Ⓐ, Ⓑ, Ⓒ, Ⓓ is crucial to correct functioning of the data-acquisition program.

At time Ⓐ the computer finishes editing data from the previous

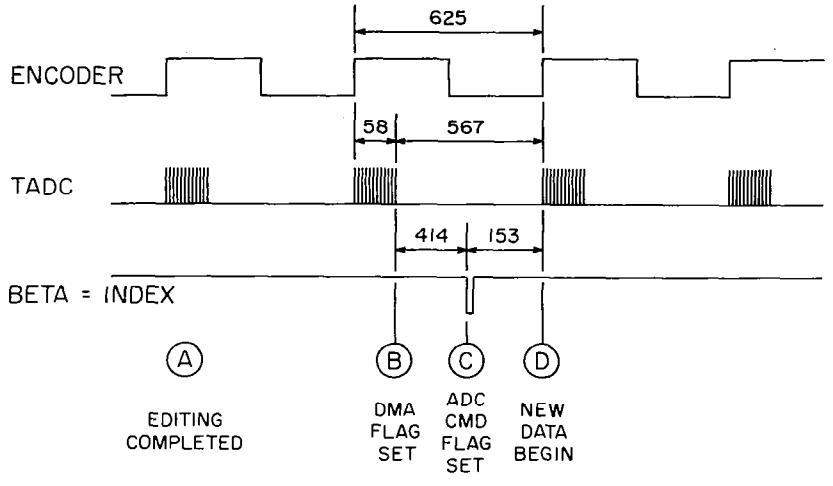

Figure 13. Timing of events at end of each revolution. Illustration is for airfoil experiment (12 analog channels; flying arm rotating at 375 rpm). Time intervals are in μsec.

revolution and enters a wait-for-flag loop to await completion of the DMA transfer for the current revolution. At time Ⓑ, when this transfer is completed, the DMA circuitry sets a flag on the DMA channel and inhibits further data transfers on the ADC data channel. During the next 414 μsec (in this example), the program first checks that the flag is still clear on the ADC command channel; i.e., that the INDEX pulse at Ⓒ has not yet occurred. If all is well, the computer checks the ADC status word to verify that the most recent word of data was in fact measured on the last analog channel, as set on the ADC front-panel toggle switches. If all is well, the program sets up the DMA circuitry for the next revolution by specifying the starting address of the alternative buffer in core and the number of words to be received (usually 3072 words, as explained above). The computer then enters a second wait-for-flag loop until an INDEX pulse occurs at time Ⓒ, setting a flag on the ADC command

channel. Beginning at time Ⓒ, the computer clears the flags on the DMA channel and the ADC command channel, activates the DMA channel and the ADC data channel, and begins editing data acquired during the revolution just completed. The first word of new data is received at time Ⓓ.

The data-acquisition process is started and stopped by means of the single control line labelled RUN in figure 12. The RUN signal is present continuously at the data input of a D-type flip-flop. This flip-flop is clocked by the INDEX pulse which occurs once per revolution when arm I of the rotor passes through the (nominal) position $\phi = -90^{o}$ (see figure 3). The system becomes armed when RUN is set true manually, and becomes latched (i.e., the flip-flop output, called BETA, goes true) when the next INDEX pulse occurs. The ADC control circuitry is designed so that a false BETA signal inhibits operation of the ADC in the automatic mode; CLOCK pulses, even if present, have no effect. However, the computer is able to manipulate the multiplexer and the ADC by internal means in order to test the voltage on any analog channel or to initialize the channel address to last channel. The BETA line also goes false momentarily at each INDEX pulse, at a time when no data are being converted. It is the fall of BETA at point Ⓒ in figure 13 which sets the flag on the ADC command I/O channel in order to inform the computer that an INDEX pulse has occurred.

The self-synchronizing properties of the data system allow a data run to be started manually at an arbitrary time after the wind tunnel and the flying arm have reached operating speed. Data from the first revolution are normally free of error. A run can be aborted (at the end of the current revolution) by setting RUN false manually. Under normal conditions, however, a run continues until the specified number of revolutions has been completed. The contents of

a revolution counter are displayed continuously on the computer front panel so that progress of the run can be monitored. At the end of a run, an end-of-file mark (EOF) is automatically written on the tape. The ADC continues to make conversions until RUN is set false, but no further DMA transfers to core memory are permitted.

The same control circuitry permits operation in an alternative mode, in which the flying arm is stationary or absent altogether. A signal generator is used to simulate rotation by supplying a regular pulse train to both the ENCODER and ZERO inputs at the controller. The program instructions which check synchronization in terms of the INDEX pulse are deleted. This mode can be used, for example, to record signals from stationary hot wires or other conventional instrumentation either for alternating blocks of 128 frames (program NOMO) or continuously (program PRESS).

5.4 Data Errors. -- Editing time is essentially fixed, independent of rotor speed, by the nature of the desired processing. At sufficiently high rotor speed, therefore, editing may still be in process when the DMA transfer is completed at time Ⓑ in figure 13, or when the INDEX pulse occurs at time Ⓒ, or even later. In such cases the only recourse is to lighten the editing task by decreasing the number of data channels, or by omitting certain editing operations (as in the STALL program), or by slowing down the flying arm. An error of this type is considered to be irrecoverable, and the computer is instructed to halt. During hot-wire calibration, for example, the upper limit imposed on rotor speed by editing requirements was about 5.0 revolutions per second. This upper limit must obviously be less than the upper limit imposed on rotor speed by power available from the PLL servo system; e.g., about 11 revolutions per second in still air, or about 6 revolutions per second at a tunnel

speed of 35 meters per second.

Two other errors in data format can occur, and in fact did occur occasionally. The first error is failure of a DMA block transfer to end on the last ADC channel. The most likely cause is electrical noise in one or another of the counting and sequencing elements in the system. The second error is occurrence of the INDEX pulse before the DMA block transfer is complete. The most likely cause is noise in the ENCODER signal from the magnetic pickup, including dropouts at low rotor speed. In either case, the data are presumably garbled. However, errors of these two types are considered to be recoverable. The program first executes a restart subroutine to reposition the multiplexer on the last channel (maximum execution time 270 μsec for 12 analog channels), and then waits for an INDEX pulse before activating the DMA channel for a new revolution. The defective data are discarded without editing. The serial number of the discarded revolution is coded for error type and recorded in a register maintained for this purpose, so that any data which are intended to be treated as a continuous time series (such as shedding phase, in the case of the vortex-shedding experiment) can be properly interpreted.

5.5 Editing. -- Each revolution of the flying arm typically involves 3072 words of data (12 channels, 256 frames). Two 3072-word data buffers in core are used alternately. During each revolution the computer edits the data obtained during the previous revolution.

There are several editing operations. In a typical case, the first eight data channels are miscellaneous signals; for example,

Tunnel dynamic pressure
Tunnel temperature
Model surface pressure
Proximity sensor peak output

Shedding phase (cylinder experiment)
Scanivalve position (airfoil experiment)
DC calibration voltages

Voltage signals from these miscellaneous channels (except the phase signals in the case of the cylinder experiment, which uses the RAMP program) are normally accumulated and averaged over the 256 frames of each revolution. The original data are discarded.

The last four channels are reserved for hot-wire data from two X-arrays, one on each arm of the rotor. For a given array, the two wire voltages are measured not quite simultaneously, but 5 μsec apart. This time interval corresponds to a probe motion of the order of 0.2 mm, or 1/5 of the wire length, and is considered to be negligible, especially as the hot-wire frequency response of 20 kHz limits the resolution of the wires to fluctuations having a period of 50 μsec or more.

Two of the data-acquisition programs, MSTRY (used mainly for hot-wire calibration) and NOMO (used mainly for pressure signals with simulated rotation), work in the same way. An INDEX pulse, occurring when the rotor arm is approximately horizontal, defines the beginning of each full revolution. During each (real or simulated) half revolution, the editing program saves verbatim the data from the X-array which is currently advancing into the airstream, and discards the data from the X-array which is currently retreating. The latter array is usually moving in the wake of its own arm, or in the flow field and wake of the large strut which supports the rotor in the test section, or both.

Provided that all wires are present and working, there are therefore two independent observations of the flow over the same 180° arc during each revolution. The data after editing consist of 512 wire voltages together with

eight mean values for the miscellaneous signals already described. These eight values are sometimes written over the first eight wire voltages, which have little significance because the active probe at this time is passing through the wake of the rotor hub.

A secondary editing operation is transfer of the 512 surviving data words to the appropriate position in one of two tape buffers, and supervision of output to magnetic tape via a second DMA channel. Four revolutions are usually combined into one tape record of 2K = 2048 words.

For each of the 128 active frames of a revolution, and for each wire of the active X-array, the program accumulates the wire voltage and its square during a run, and also records the largest and smallest voltages observed since the beginning of the run. When a run is finished (a file may contain data from as few as 64 or as many as 4096 revolutions and may require from a few seconds to 15 minutes of tunnel time), the program determines for each frame and each active wire the mean voltage, the rms voltage fluctuation, and the maximum and minimum voltage during the file. The results are written on tape as a terminal record which can be dumped and inspected almost immediately to verify correct operation of the data system. The information in the last record can obviously also be reconstituted from the verbatim records recorded throughout a run. The program sections which generate the last record are therefore considered expendable; they account for roughly half of the editing time and were deleted in the STALL program to reduce editing time at high rotor speeds. A 128-word appendix to the terminal record includes a list of the format parameters for the run (ID, NREV, etc.) and a list of the serial numbers of any revolutions discarded during the file. The terminal record is therefore normally 2048 + 128 = 2176 words.

Another data-acquisition program, RAMP, is designed specifically for the cylinder experiment. In particular, the first two analog data channels are ramp signals representing the phase of the vortex-shedding process (see reference 2). A shortage of core space limited the number of active frames (i.e., frames for which hot-wire data could be recorded as time series) to 78 frames out of 128. The data for each revolution therefore include 4 x 78 = 312 words of hot-wire voltages, 256 words of ramp data (as continuous time series through an entire file, with the two ramp signals combined in a single word per frame), and eight mean values for miscellaneous signals (with the ramp channels recorded as zero), for a total of 576 words per revolution or 4 x 576 = 2304 words per tape record. The format of the terminal record is unchanged; in particular, mean, rms, max, and min voltages are recorded for all 128 frames of each half revolution.

These data-acquisition programs can be (and sometimes were) used in a non-standard mode by interchanging analog signals, since editing is programmed by channel rather than by signal.

The registers which accumulate voltage and squared voltage for each wire during a file are double-word and triple-word registers respectively. The programs were never developed to the point of incorporating the full multiple-precision 2's-complement binary arithmetic necessary to cope with both positive and negative integers. Voltages directed to any one of these accumulators are required to be always positive or always negative. In the latter case they are made positive before accumulation, and the negative sign is restored after calculation of the mean value. This restriction is not a serious one in practice.

In summary, as far as data rate is concerned, the ADC operates at

200, 000 words per second in a synchronous burst mode. The computer typically acquires data asynchronously at an average rate of about 18, 000 words per second (for a rotor speed of 360 rpm). After editing, the magnetic tape transport records data at an average rate of about 3, 000 words per second. The recorded data base for the airfoil experiment (reference 1) amounts to about 80, 000, 000 words, and for the cylinder experiment (reference 2) amounts to about 400, 000, 000 words.

VI. HOT-WIRE CALIBRATION

6.1 Digital Anemometry. -- The self-calibrating property of the flying hot wire has been discussed in principle in sections 2.1 and 2.2 above. When principle is reduced to practice, several special problems arise which are not typical of the ordinary art of hot-wire anemometry. First, the flying probe operates at velocities roughly twice the flow velocities of interest. The resulting loss of wire sensitivity increases the error in measurement of flow direction and velocity, and this error is further amplified during conversion of data from a moving to a fixed frame. Second, the flying probe, being intended for use in highly turbulent flow, requires calibration over larger ranges of velocity than is normal with fixed probes. Third, the probe calibration arc involves a considerable fraction of the tunnel test section, and non-uniformities of the calibration flow along this arc may be quite important. These problems indicate a need for unusually tight control of wire calibration.

For a fixed operating condition, the two wire voltages for an X-array in steady two-dimensional flow depend only on two relative velocity components (U and V, say) in the plane of the array. Schematically,

$$e_1 = e_1(U, V; P_1) \tag{11a}$$

$$e_2 = e_2(U, V; P_2) \tag{11b}$$

where P is a set of fixed parameters characterizing the response of the particular wire. In the present research, a quasi-steady two-dimensional approximation is also made by taking the corresponding inversion formulas,

$$U = U(e_1, e_2; P_1, P_2) \tag{12a}$$

$$V = V(e_1, e_2; P_1, P_2) \tag{12b}$$

to be unique. Either pair of variables (U, V) or (e_1, e_2) is assumed to determine the other at all times. Effects of wire separation, finite wire length, fast fluctuations, steep gradients, large signal amplitudes, the unknown third velocity component, and the like are treated as negligible, at least compared to larger experimental objectives of the research.

These schematic relationships have to be made specific. The experience of many investigators has established that the behavior of a given wire can be adequately represented by an empirical formula known as King's law,

$$Nu = a + b(Re_e)^{\eta} \tag{13}$$

By definition,

$$Nu = \frac{e^2}{\pi L k R \Delta T} \tag{14}$$

and

$$Re_e = \frac{\rho q_e d}{\mu} \tag{15}$$

where q_e is some effective cooling velocity, e is wire voltage, ΔT is temperature loading ($T_{wire} - T_{air}$), R is wire hot resistance, L and d are wire length and diameter, ρ, k, and μ are air density, heat conductivity, and viscosity, and a, b, and η are fixed wire parameters of the kind

previously denoted by P.

In the present application the hot wire is viewed simply as a measuring tool, and there is no reason to think of King's law as a universal relationship or even as a non-dimensional one. Several of the quantities used to form Nu and Re, such as L and d, are constant for a given wire and can be suppressed. In the constant-temperature mode of operation R does not change, and ΔT changes only if T_{air} does. If the fluid properties ρ, k, and μ can be evaluated at the wire hot temperature, they also become constant (except for the dependence of ρ on pressure). In dimensional form, therefore, equations (11) for the behavior of the two wires of an array become

$$N_1 = \frac{e_1^2}{\Delta T_1} = A_1 + B_1(q_{e_1})^{\eta_1} \tag{16a}$$

$$N_2 = \frac{e_2^2}{\Delta T_2} = A_2 + B_2(q_{e_2})^{\eta_2} \tag{16b}$$

where now A, B, and η are wire parameters.

The two processes of hot-wire anemometry are calibration and inversion. Once q_e has been defined in terms of two velocity components U and V relative to the probe body, calibration consists of varying U and V, recording the two wire voltages e_1 and e_2, and determining the wire parameters--for each wire separately--by a fit of the data to some analytical formula such as equations (16).

There remains the problem of inversion, as represented schematically by equations (12). The essence of digital anemometry is that the inversion process may be carried out many millions of times in a digital computer. The literature of the subject does not emphasize the fact that a poor definition for q_e may stultify this inversion process. To see the difficulty, it is useful to

think of the two velocities q_e as the primary stuff of inversion. On the one hand, these velocities are essentially measured quantities, since from (16),

$$q_{e_1} = \left(\frac{N_1 - A_1}{B_1}\right)^{1/n_1} \tag{17a}$$

$$q_{e_2} = \left(\frac{N_2 - A_2}{B_2}\right)^{1/n_2} \tag{17b}$$

Given King's law, the calculations involved in equations (17) are not under the control of the experimenter. On the other hand, the velocities q_e are also by assumption expressible in terms of U and V. Computing costs can increase dramatically if the analytical form for $q_e(U, V)$ is poorly chosen. It goes almost without saying that the inversion formulas should be soluble for U and V in closed form, without linearization or other approximation. In particular, iteration schemes of whatever kind should be avoided. *

Several choices have been proposed in the literature of hot-wire anemometry for the effective cooling velocity q_e. The traditional choice is to take q_e as the component q_n of velocity normal to the wire,

$$q_e = q_n \tag{18}$$

If another degree of freedom is desired, an alternative choice (see the discussion by Champagne et al. in reference 5) is to include a small contribution to cooling from the velocity component q_p parallel to the wire,

$$q_e = (q_n^2 + \kappa^2 q_p^2)^{1/2} \tag{19}$$

---

*Exceptions to this rule can occur. For example, if the data base is sufficiently massive, it may be efficient to implement the inversion operation by tabular lookup. A limited form of this latter strategy was in fact used in the cylinder experiment (reference 2).

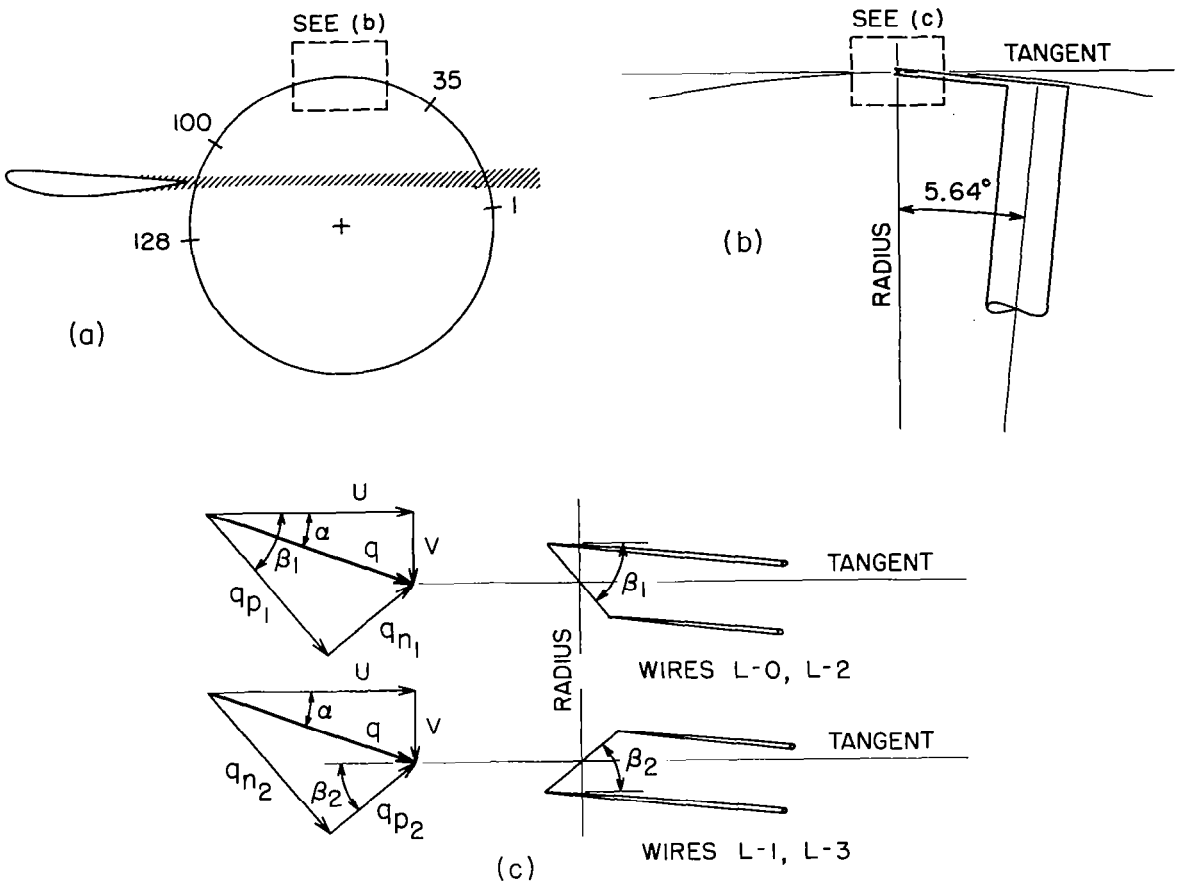

Figure 14. Further details of probe geometry, including notation for relative velocity components.

(a) Probe trajectory for wire calibration during airfoil experiment. Flow is from left to right, with airfoil at zero lift. Probe rotation is counter-clockwise. Location of frames 1, 35, 100, 128 is marked on calibration arc.

(b) Closeup view of rotor tip showing probe angular offset of 5.64°.

(c) Resolution of relative velocity (q) into tangential (U) and radial (V) components with respect to probe circle, and also into normal (q_n) and parallel (q_p) components with respect to wires. All quantities are positive as shown.

The formulas (18) and (19) are not equivalent from the point of view of inversion. If q_e is defined by (18), then in the notation of figure 14c (in which

U and V denote tangential and radial components, with the same sign convention as in section 2.1 above),

$$q_{e_1} = q_{n_1} = U \sin\beta_1 - V \cos\beta_1 \tag{20a}$$

$$q_{e_2} = q_{n_2} = U \sin\beta_2 + V \cos\beta_2 \tag{20b}$$

where β is also a wire parameter. The system (17), (20) is recognizable as a parametric form of the general inversion equations (12). Inversion consists of calculating q_{e_1} and q_{e_2} from equations (17) and then solving the two linear algebraic equations (20) for U and V. Note that the wire parameters fall naturally into two groups; only A, B, and η enter into the first calculation, and only β (and also n and C, if used) into the second one.

Matters are more complicated when the effective cooling velocity is defined by (19). Two additional relationships from figure 14c are

$$q_{p_1} = U \cos\beta_1 + V \sin\beta_1 \tag{21a}$$

$$q_{p_2} = U \cos\beta_2 - V \sin\beta_2 \tag{21b}$$

Inspection of (21), (20), and (19) shows that inversion now requires the solution of two quadratic algebraic equations for U and V. In terms of computing efficiency, therefore, (19) runs a poor second to (18).

In the present research, the preferred choice for q_e is neither (18) nor (19), but

$$q_e = q_n + C \tag{22}$$

where now C is an additional wire parameter. Let the flow relative to the probe be defined by the magnitude and direction of the velocity; i.e., by $q = (U^2 + V^2)^{1/2}$, $\alpha = \arctan(V/U)$, as in figure 14c, and take $q_e = q_n$ for simplicity. Then King's law can be rewritten as

$$N = A + B'(\alpha) q^{\eta} \tag{23}$$

where

$$B'(\alpha) = B \sin^{\eta}(\beta \pm \alpha) \tag{24}$$

In coordinates (q^{η}, N), therefore, calibration data for a given wire for various fixed values of α are necessarily fitted to a fan of straight lines passing through the point (0, A) with slope $B'(\alpha)$, as indicated in figure 15a. Especially when the range of q is large, our experience has been that another degree of freedom is desirable, and that a better fit can be obtained if the fan originates at a point off the N axis, as indicated in figure 15b. The required modification to King's law is

$$N = A + B'(\alpha)(q^{\eta} + c) \tag{25}$$

where c is defined in the figure. An equivalent statement to (25) is

$$q_e = q_n \left(1 + \frac{c}{q^{\eta}}\right)^{1/\eta} \tag{26}$$

This choice (26) for q_e is highly regressive, because solution for U and V can be accomplished only by iteration. The much simpler choice (22) is

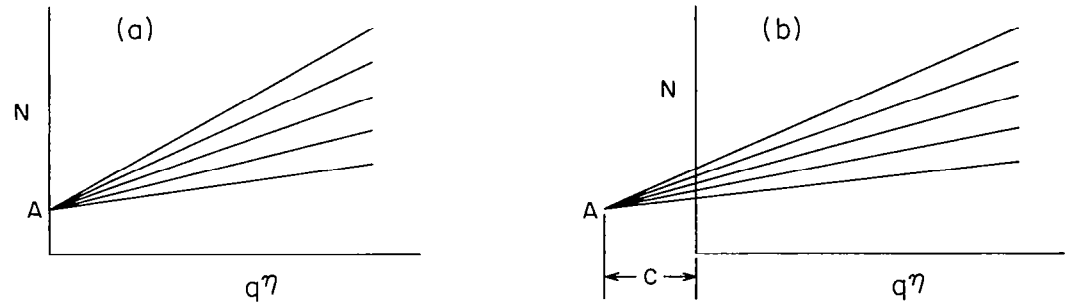

Figure 15. Experience with King's law.
(a) Conventional form described by equation (23).
(b) Proposed modification described by equation (25).

proposed as an empirical imitation of (26) which provides a nearly equivalent additional degree of freedom and at the same time preserves the advantage of linear algebra during inversion.

6.2 Sample Probe Calibration. -- A typical (i.e., best) probe calibration from the body of the present research is the post-test calibration for the airfoil experiment. The airfoil model was quite complex, and its removal from the wind tunnel during probe calibration was not practicable. Instead, the best available approximation to uniform flow was obtained by pitching the airfoil to its angle of attack for zero lift, namely -4°. To minimize any residual effect of the narrow airfoil wake, the probe traverse was moved as far downstream as possible and then elevated until the probe just missed the trailing edge. The resulting geometry during probe calibration is shown in figure 14a.

For each tunnel dynamic pressure used in the calibration (nominal values 1, 2.5, 5, 10, 15, 20 lbf/ft^2), the magnitude of the free-stream velocity was determined at six points along the calibration arc by clamping the rotor arm and substituting a conventional pitot-static tube for one hot-wire probe. Data from the pitot-static tube covered the range $-40^{\circ} < \phi < +50^{\circ}$ (ϕ is defined in figure 1), corresponding to data frames 35-100 (of 1-128). For interpolation purposes, the measured dynamic pressure along this portion of the calibration arc was fitted for each tunnel condition to a 4th degree polynomial in the downstream coordinate. The accuracy of fit was about one part in 10^3 in local velocity.

Figure 16 shows raw calibration data for one wire array (wires L-1, L-0, or "last channel minus one", "last channel minus zero") in the form N_1 against N_0. The operating conditions for the flying arm and for the tunnel are

listed in table 1. The data in the figure are mean values for 256 revolutions, and a typical trace represents from 70 to 250 seconds of tunnel operation, depending on rotor speed. However, the complete calibration required about 110 minutes, most of which was spent in changing tunnel dynamic pressure and waiting for tunnel equilibrium.*

Table 1

Operating conditions for wind tunnel and probe for post-test calibration during airfoil experiment.

MSET	Octal ID	Nominal dynamic pressure (lbf/ft^2)	u_∞ (m/sec)	ωR (m/sec)	K
1	2217	1	9.56	4.96	0.52
2	2220	1	9.59	6.76	0.70
3	2221	1	9.57	9.29	0.97
4	2222	2.5	14.19	9.29	0.65
5	2223	2.5	14.20	6.76	0.48
6	2224	5	20.30	6.09	0.30
7	2225	5	20.47	8.85	0.43
8	2226	5	20.23	11.99	0.59
9	2227	10	29.37	11.44	0.39
10	2230	10	29.37	8.45	0.29
11	2231	15	36.21	10.62	0.29
12	2232	15	36.28	13.52	0.37
13	2233	20	42.06	11.99	0.29
14	2234	20	42.09	17.70	0.42

*The table shows a clear violation of the second law, "skip around". (The first law is "turn one knob at a time".) This probe calibration occurred near the end of a long and exhausting test session, and the tunnel dynamic pressure was increased monotonically simply to minimize the chance of wire breakage early in the calibration. At the end of the calibration, the run MSET 4 was duplicated as MSET 15. Three of the wires showed no appreciable change in properties; wire L-2 shifted slightly (N changed by 0.002 for fixed q_e).

The platinum-plated tungsten wires were mounted at a nominal angle of $\pm 45^{\circ}$ to the probe axis. The wire diameter was 5 μm and the wire length was about 1 mm. Typical wire voltages were in the range 5 to 8 volts. The operating resistance ratio was about 1.4, corresponding to a temperature loading ΔT of about $110^{\circ}C$. Hence the quantity $N = e^2/\Delta T$ has the units $volts^2/^{\circ}C$ and falls in the range 0.3 to 0.6. The units for q, q_e, etc. are always m/sec in what follows.

Probe motion is from right to left along each trace in figure 16. The strong disturbance at the left in several of the traces is caused by passage of the probe through the airfoil wake close to the trailing edge, at frames 110-114 (cf. figure 14a). The traces in question are all for relatively high rotor speeds, with values of $K = \omega R/u_{\infty}$ from 0.43 to 0.97. According to section 2.1 and figure 8, larger K means that a larger arc is traversed by the probe before the relative flow becomes momentarily parallel to one of the wires and the trace turns back on itself. The third trace, for which $K = 0.97$, also shows a detectable disturbance at the right caused by passage of the probe through the wake of the preceding rotor arm. These disturbances are all outside the range of present interest.

The data used for wire calibration are from frames 35-100. For economy, only even-numbered frames are processed. Any frames for which the flow angle relative to the probe falls outside the range $\pm 30^{\circ}$ (this angle is now measured from the bisector of the angle between the two wires of an array) are discarded at an intermediate stage of processing. The behavior of one wire, L-1, is typical and is reported in detail.

As a first approximation, the flow direction in the free stream is assumed to be parallel to the tunnel axis. Equation (22) defines the effective

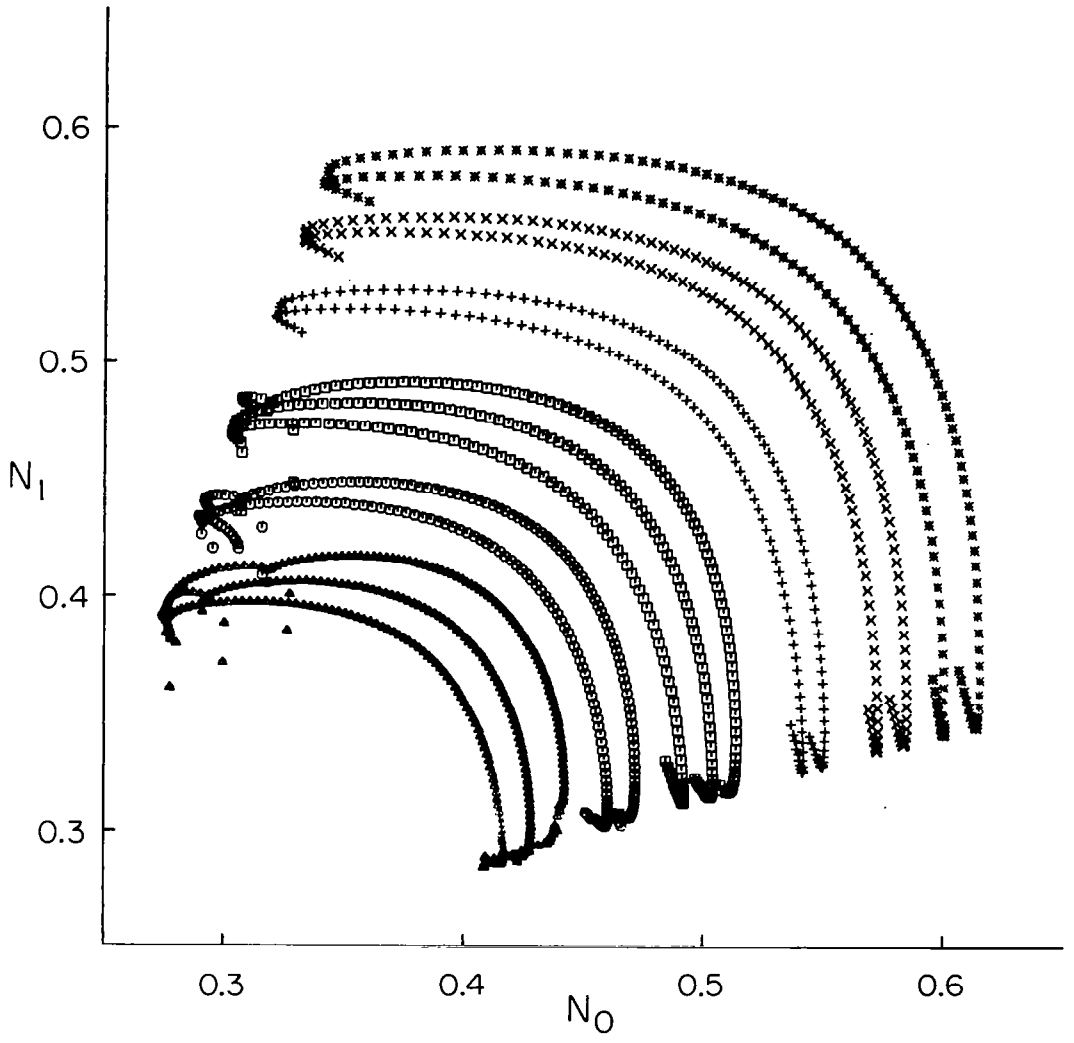

Figure 16. Raw data from one X-array (wires L-1, L-0) for post-test calibration during airfoil experiment. Quantity $N = e^2/\Delta T$ is dimensional, with units of volts^2/$^\circ$C. Six different symbols refer to six different values for tunnel dynamic pressure. Sequence of traces is same as in table 1 except for MSET 4-5 and MSET 9-10.

cooling velocity. Figure 17a shows the quality of fit obtained for wire L-1 when A, B, η, β, and C are chosen to minimize the dispersion in N for the calibration taken as a whole. The left trace (MSET 1) is correctly placed

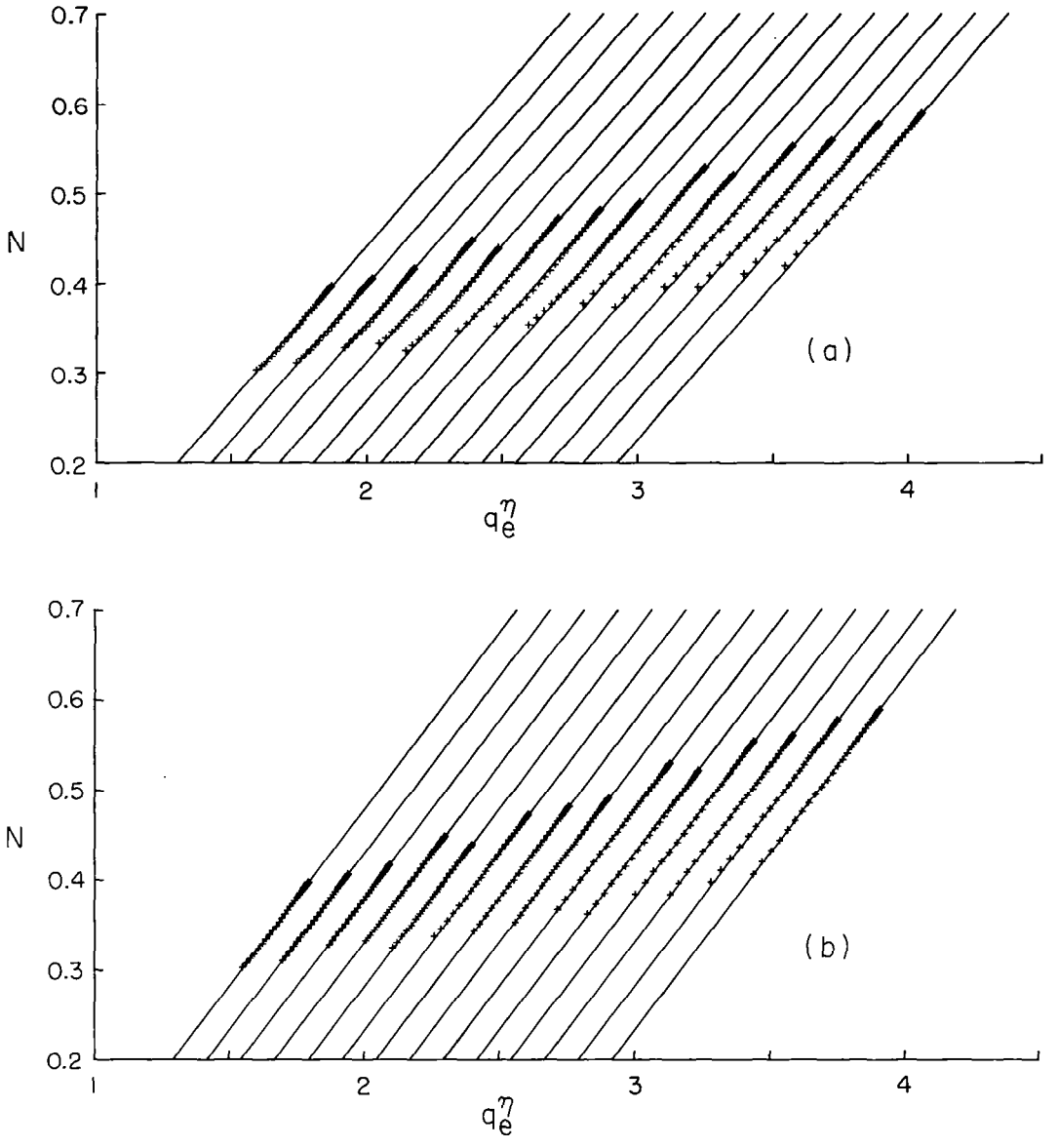

Figure 17. Calibration data for wire L-1 in coordinates of King's law. Effective cooling velocity is $q_e = q_n + C$. Ambient flow velocity q is taken from pitot-static measurements. Sequence of traces is same as in table 1. Scales apply to first trace at left; other traces are displaced by 0.125 in abscissa.

(a) Ambient flow direction is assumed parallel to tunnel axis.

(b) Ambient flow direction is corrected by bootstrap procedure, using inverted calibration data (two iterations).

in the coordinates of the figure; the other traces are successively displaced by increments of 0.125 in the abscissa. All of the traces show a consistent small discrepancy between the data and the common straight line. On the supposition that this discrepancy is caused by variations in free-stream flow direction, the discrepancy can be reduced by a bootstrap procedure in which the calibration itself is used to redefine the free-stream flow.

The result of the bootstrap procedure is illustrated for one dynamic pressure (nominally 10 lbf/ft^2) in figure 18. When the calibration data are inverted, four (sometimes six) independent observations of the flow are available, corresponding to two probe arrays and to two (sometimes three) rotor speeds. The bootstrap consists of replacing the original values for free-stream flow direction, $\theta = \tan^{-1}(v/u)$, by the average of the observations, as shown by the solid line in figure 18. The original pitot-static values for free-stream

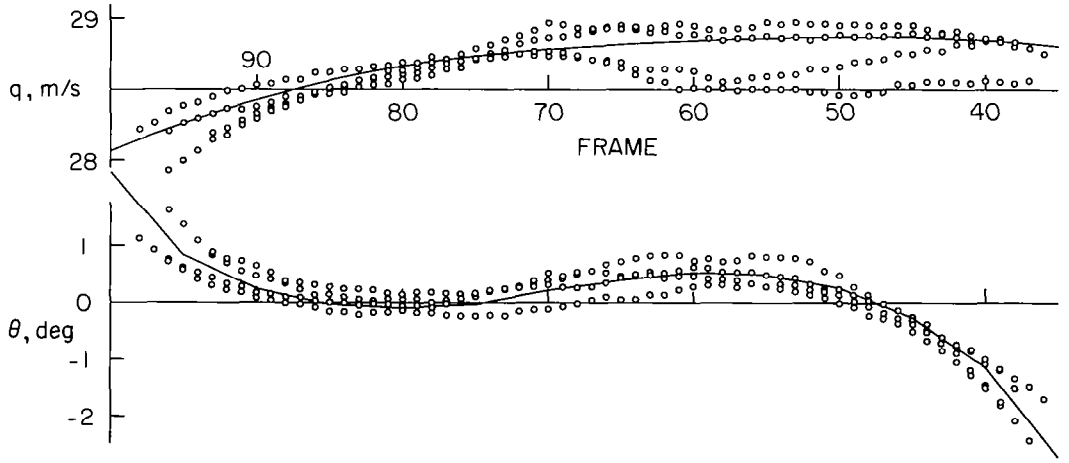

Figure 18. Use of bootstrap procedure to determine ambient flow (solid lines) by inversion of calibration data. Four observations plotted are for two probe arrays at two values of K at one dynamic pressure (nominally 10 lbf/ft^2). Discrepancies of one to two percent in velocity and one degree in angle are typical of entire calibration.

velocity q, also shown by a solid line, are left undisturbed. The calibration procedure is then repeated with this revised free-stream flow. Two iterations are sufficient for adequate convergence. For the final calibration fit, shown in figure 17b, the dispersion in N is reduced by more than a factor of two compared to figure 17a.

It is by no means certain that this bootstrap procedure is correct. The procedure may simply compensate for imperfections in the formula used to define effective cooling velocity as a function of relative flow direction. Moreover, the procedure is only capable of giving information about the AC component of flow inclination. Any DC component will be incorporated into the calculated wire angles β and hence will be undetectable in the data. In any event, the indicated correction is found to be similar for both probes and almost independent of tunnel dynamic pressure.

Finally, table 2 examines the relative merit of the various definitions for effective cooling velocity q_e as discussed in section 6.1. Again, only wire L-1 is considered. The ambient flow (with bootstrap, as in figure 18) and the experimental data are the same in all four cases. The only difference is the presence or absence of the parameters $\varkappa$ and C in the composite definition

$$q_e = (q_n^2 + \varkappa^2 q_p^2)^{1/2} + C \qquad (27)$$

which reduces to (18), (19), or (22) as appropriate. The parameters A, B, η, and β (and $\varkappa$ and C if present) are again determined simultaneously by a fit which minimizes the dispersion σ for the dependent variable N in King's law.

Table 2 shows that the effect of including the parameter $\varkappa$ (displacement to the right in the table) is to reduce the dispersion in N, with little

Table 2

Influence of $\varkappa$ and C on wire parameters for wire L-1. Ambient flow is defined by bootstrap procedure. Effective cooling velocity is

$$q_e = (q_n^2 + \varkappa^2 q_p^2)^{1/2} + C$$

		$\varkappa = 0$	$\varkappa \neq 0$
$C = 0$	A	0.1458	0.1408
	B	0.0935	0.0974
	η	0.3989	0.3921
	β	0.5885	0.5728
	$\varkappa$	—	0.0898
	C	—	—
	σ	0.00107	0.00096
$C \neq 0$	A	-0.3079	-0.3044
	B	0.3932	0.3943
	η	0.2057	0.2046
	β	0.5880	0.5711
	$\varkappa$	—	0.0929
	C	5.104	4.842
	σ	0.00076	0.00057

change in the remaining wire parameters. The effect of including the parameter C (displacement downward in the table) is also to reduce the dispersion in N, but with quite large changes in all of the remaining wire parameters except β. In particular, the intercept A becomes negative, and the exponent η decreases from about 0.4 to about 0.2. The dispersion in N is evidently least when both $\varkappa$ and C are different from zero. However, the case $\varkappa \neq 0$ is subject to the algebraic difficulties already described in section 6.1.* The

*Wire L-1 is the only one of the four wires for which the optimum value for $\varkappa$ (~ 0.09) is large enough to be significant. It is mainly for this reason that wire L-1 is selected for discussion in the text.

final parameters assigned to wire L-1 are therefore the ones enclosed in the box in table 2. These are also the parameters used to produce figure 17b.

One minor disadvantage of the new proposal $q_e = q_n + C$ is that the sensitivity of q_n to errors in N is slightly increased compared to the case $C = 0$. From equations (17) and (22), with A, B, C, and η fixed, the sensitivity in question is

$$S = \frac{d\ell n q_n}{d\ell n N} = \frac{1}{\eta}\left(\frac{N}{N - A}\right)\left(\frac{q_n + C}{q_n}\right) \tag{28}$$

The range of q_n covered by the present calibration is quite large. At the low end, $q_n \sim 3$ and $N \sim 0.3$ (units are m/sec and volts^2/$^\circ$C respectively). At the high end, $q_n \sim 50$ and $N \sim 0.6$. These values, together with the entries in table 2 for $\varkappa = 0$, yield values for S in the range 3 to 5 for $C = 0$ and in the range 4 to 7 for $C \neq 0$. For the parameters enclosed in the box, the dimensionless dispersion in N is roughly $\Delta N/N \sim 0.00076/0.45 \sim 0.0017$. Hence the expected error using this calibration is about one percent in relative velocity and about two percent in absolute velocity. This estimate is consistent with the data for q in figure 18. The error in flow inclination θ is not known, since this quantity was not measured independently. However, the flow angles inferred from the calibration are usually repeatable within one degree or better, as demonstrated for one dynamic pressure in figure 18.

In the present work the useful angular range of the X-wire probes is taken as $\pm 30^\circ$. In any attempt to increase this range toward the theoretical limit of $\pm 45^\circ$ for such probes, the proposal (22) for q_e must be abandoned or at least modified. The reason is that this equation requires q_e to be an absolute constant when $q_n = 0$. It follows from equations (16) that the heat transfer N is also an absolute constant. Figure 8 confirms that the observed

minimum in e or N occurs at or very close to the position where q_n vanishes. Consequently, the envelope of the various traces in figure 16 is known to correspond to the condition $q_n = 0$. But on this envelope N is certainly not an absolute constant; it depends on the overall velocity level for the trace in question, and in particular on q_p (in reference 3, this dependence is used to determine $\varkappa$). This argument favors equation (19) or perhaps equation (27) over equation (22) if the primary objective is to increase the angular range of a standard X-array without regard to computing cost. However, the simplest and cheapest way to increase the angular range of an X-array, or to improve the overall accuracy for a fixed angular range, is simply to mount the wires more nearly normal to the flow, inclined (say) at 60° to the probe axis rather than 45°. Nothing in the analytical or experimental techniques of hot-wire anemometry, analog or digital, would change in any important respect. Perhaps X-arrays are made the way they are because they have always been made that way.

REFERENCES

1. Wadcock, A. A flying-hot-wire study of two-dimensional flow past an NACA 4412 airfoil at maximum lift. Ph. D. Thesis, California Institute of Technology, 1977.

2. Cantwell, B. A flying-hot-wire study of the turbulent near wake of a circular cylinder at a Reynolds number of 140, 000. Ph. D. Thesis, California Institute of Technology, 1975.

3. Tutu, N. and Chevray, R. Cross-wire anemometry in high intensity turbulence. Journal of Fluid Mechanics 71, 785-800, 1975.

4. Perry, A. and Morrison, G. A study of the constant-temperature hot-wire anemometer. Journal of Fluid Mechanics 47, 577-599, 1971.

5. Champagne, F., Sleicher, C., and Wehrmann, O. Turbulence measurements with inclined hot-wires. Part 1. Heat transfer experiments with inclined hot-wire. Journal of Fluid Mechanics 28, 153-175, 1967.

1. Report No.	2. Government Accession No.	3. Recipient's Catalog No.
CR-3066		

4. Title and Subtitle	5. Report Date
The Flying Hot Wire and Related Instrumentation	November 1978
	6. Performing Organization Code

7. Author(s)	8. Performing Organization Report No.
Donald Coles, Brian Cantwell, and Alan Wadcock	
	10. Work Unit No.

9. Performing Organization Name and Address	11. Contract or Grant No.
Graduate Aeronautical Laboratories California Institute of Technology Pasadena, CA 91125	NGL 05-002-229
	13. Type of Report and Period Covered
12. Sponsoring Agency Name and Address	Contractor Report
National Aeronautics and Space Administration Washington, D. C. 20546	14. Sponsoring Agency Code

15. Supplementary Notes

16. Abstract

A flying-hot-wire technique is proposed for studies of separated turbulent flow in wind tunnels. The technique avoids the problem of signal rectification in regions of high turbulence level by moving the probe rapidly through the flow on the end of a rotating arm. New problems which arise include control of effects of torque variation on rotor speed, avoidance of interference from the wake of the moving arms, and synchronization of data acquisition with rotation. Solutions for these problems are described. The self-calibrating feature of the technique is illustrated by a sample X-array calibration.

17. Key Words (Suggested by Author(s))	18. Distribution Statement
Flow measurement Separated flow Hot-Wire Anemometers Data Systems	UNCLASSIFIED-UNLIMITED STAR - Category 34

19. Security Classif. (of this report)	20. Security Classif. (of this page)	21. No. of Pages	22. Price*
UNCLASSIFIED	UNCLASSIFIED	62	$5.25

*For sale by the National Technical Information Service, Springfield, Virginia 22161

NASA-Langley, 1978